Wu *et al.*
European Journal of Medical Research (2026) 31:91
https://doi.org/10.1186/s40001-025-03667-0

European Journal of Medical Research

RESEARCH

Open Access

Multimodal analysis reveals potential association of CDH13 with endothelial cells and its overexpression in hepatocellular carcinoma

Ke-Jun Wu[1†], Li-Hua Yang[2†], Dong-Ming Li[1], Rong-Quan He[2], Di-Yuan Qin[3], Shi-De Li[1], Jian-Di Li[1], Yi-Wu Dang[1], Ming-Jie Li[1], Qi Li[1], Jian-Jun Li[4], Lu Zhang[1], Han He[1], Ji-Feng He[1], Gang Chen[1*] and Xiao-Bo Jiang[5*]

Abstract

Background Hepatocellular carcinoma (HCC) is the fourth leading cause of cancer-related death worldwide and shows significant heterogeneity. Cadherin 13 (CDH13) is abnormally expressed in various malignancies, but its role in HCC and the tumor microenvironment remains unclear.

Objective This study aimed to systematically explore the expression, regulatory mechanisms, and potential functions of CDH13 in HCC using a multi-omics strategy.

Methods We integrated transcriptomics, proteomics, spatial transcriptomics, single-cell RNA sequencing (scRNA-seq), immunohistochemistry (IHC), clustered regularly interspaced short palindromic repeats/CRISPR-associated protein 9 (CRISPR/Cas9) gene editing, chromatin immunoprecipitation sequencing (ChIP-seq), weighted gene co-expression network analysis (WGCNA), gene set variation analysis (GSVA), immune infiltration analysis, molecular docking, phenotypic analysis, and survival analysis.

Results In multiple cohorts, CDH13 mRNA was significantly upregulated in 5145 HCC samples (standardized mean difference (SMD) = 1.17) and associated with poor prognosis (hazard ratio (HR) = 2.06). Protein levels were elevated in 165 public and 476 clinical paired samples (361 from Guangxi Medical University, 115 from Yulin Red Cross Hospital; SMD = 2.48), mainly localized to the cytoplasm and membrane. Spatial transcriptomics showed CDH13 enrichment in tumor regions and spatial association with endothelial cells, which was confirmed in an independent HCC tissue section. Focusing on cell function, CRISPR/Cas9 knockout of CDH13 significantly inhibited proliferation in HCC cell lines such as SNU182, SNU739, HUH7, etc. Further analysis showed CDH13 was expressed in hepatocytes, endothelial cells, and hepatitis B virus (HBV)-infected regions; pseudotime analysis indicated late-stage upregulation in endothelial cells and activation of the macrophage migration inhibitory factor (MIF) pathway. IHC confirmed moderate CDH13 positivity in tumor cells and strong positivity in microvascular endothelial cells. CDH13-high endothelial cells were

†Ke-Jun Wu and Li-Hua Yang have contributed equally as first authors.

*Correspondence:
Gang Chen
chengang@gxmu.edu.cn
Xiao-Bo Jiang
jiang_xiaobo_gx@163.com
Full list of author information is available at the end of the article

enriched in pyrimidine metabolism, oxidative phosphorylation, and propanoate metabolism. WGCNA and GSVA linked CDH13-related genes to angiogenesis, invasion, and metabolic reprogramming. ChIP-seq identified binding of Forkhead box A1 (FOXA1) to CDH13 regulatory regions. Clinically, CDH13 negatively correlated with regulatory T cells (Tregs, R = −0.311) and γδ T cells (R = −0.206), and positively with stromal scores (R = 0.400). High CDH13 predicted poor immunotherapy response (Area Under the Curve (AUC) = 0.745–0.795) and prognosis. Molecular docking shows a binding with docetaxel (−7.6 kcal/mol), while phenotypic analysis showed no obvious physiological toxicity.

Conclusion CDH13 is highly expressed in HCC and may promote angiogenesis, immune evasion, and metabolic reprogramming via the FOXA1-CDH13 axis, suggesting its potential as a therapeutic target.

Keywords CDH13, Hepatocellular carcinoma, Endothelial cells, Angiogenesis, CRISPR/Cas9

Introduction

HCC is one of the most common primary malignant tumors of the liver worldwide and ranks as the fourth leading cause of cancer-related death [1] The development of HCC is closely associated with chronic liver diseases, including HBV infection, alcoholic liver disease, and nonalcoholic fatty liver disease. Although advances in imaging diagnosis, surgical resection, liver transplantation, and targeted therapies [2] (such as sorafenib and lenvatinib) have improved survival in some patients, the 5-year survival rate of HCC remains low, mainly due to its high heterogeneity and metastatic potential [3]. Therefore, exploring the molecular mechanisms of HCC and identifying novel diagnostic markers and therapeutic targets are crucial for improving patient prognosis.

CDH13 is an atypical cadherin widely expressed in endothelial cells, neurons, cardiomyocytes, and other tissues [4, 5]. Unlike classical cadherins, CDH13 is anchored to the cell membrane via a glycosylphosphatidylinositol (GPI) anchor[6], lacking transmembrane and cytoplasmic domains, and mainly functions as a signaling molecule regulating intercellular communication[7], angiogenesis[8, 9], and cell migration[9]. Studies have shown that CDH13 is abnormally expressed in multiple malignancies, such as breast cancer [10] and adrenocortical carcinoma [4], and is associated with tumor invasion, metastasis, and prognosis. In HCC, high promoter methylation of CDH13 in peripheral blood mononuclear cells (PBMCs) is associated with decreased mRNA expression and poor prognosis, suggesting its potential as a non-invasive biomarker for diagnosis and prognostic evaluation [11]. However, that study was limited by a relatively small sample size (157 HCC patients) and mainly focused on HBV-related HCC, without sufficient representation of other etiologies such as hepatitis C virus (HCV) infection or nonalcoholic fatty liver disease, which may limit the generalizability of its conclusions. Moreover, it only analyzed methylation in PBMCs without exploring the methylation patterns of CDH13 in tumor tissues or its interaction with the tumor microenvironment, requiring further investigation to validate its specificity and sensitivity as a biomarker. Nevertheless, the potential dysregulation of CDH13 and its interaction with the tumor microenvironment in HCC provide important scientific clues for its role as a diagnostic and therapeutic target.

Endothelial cells are key components of the HCC tumor microenvironment and play critical roles in tumor angiogenesis, nutrient supply, and immune cell recruitment. The highly vascularized nature of HCC [12] makes it heavily dependent on endothelial cell function, while metabolic reprogramming and aberrant signaling in these cells (e.g., through Vascular endothelial growth factor (VEGF)[13]or MIF [14] pathways) further promote tumor progression. The high expression of CDH13 in endothelial cells may influence the formation of an immunosuppressive microenvironment in HCC by modulating cell adhesion, signal transduction, and metabolic pathways, thereby affecting the efficacy of immunotherapies such as anti- programmed death protein 1(PD-1)/programmed deathligand 1(PD-L1) treatment. ScRNA-seq and spatial transcriptomics [15] provide powerful tools to elucidate the role of CDH13 in the HCC microenvironment. Spatial transcriptomics preserves tissue spatial context while enabling high-resolution gene expression profiling, allowing precise mapping of CDH13 expression in tumor and peritumoral regions and its spatial relationship with endothelial cells, tumor cells, and immune cells. Compared to conventional transcriptomics, spatial transcriptomics offers advantages in capturing tissue heterogeneity, cell type-specific expression, and intercellular communication networks, thus offering a unique perspective on the spatial functional characteristics of CDH13 in HCC.

In this study, we systematically explored the expression pattern, molecular mechanisms, and interactions of CDH13 within the tumor microenvironment of HCC by integrating multiple omics tools, including scRNA-seq, spatial transcriptomics, bulk RNA sequencing (RNA-seq), proteomics, and ChIP-seq. ScRNA-seq and spatial transcriptomics provide cell-type-specific and spatially resolved gene expression data, revealing

CDH13 expression within tumor regions and its interactions with endothelial and immune cells. Bulk RNA-seq and proteomics offer comprehensive insights at the gene and protein levels, enabling us to identify key molecular patterns associated with CDH13. ChIP-seq was used to identify transcription factors, such as FOXA1, that regulate CDH13 expression, uncovering the underlying transcriptional mechanisms. CRISPR/Cas9 gene editing was employed to validate the functional role of CDH13 in HCC cell proliferation. Additionally, WGCNA and GSVA were applied to uncover co-expression relationships and enriched biological pathways related to CDH13, highlighting its role in angiogenesis and metabolic reprogramming. These tools were chosen for their ability to provide complementary, multi-dimensional insights into CDH13's involvement in HCC, offering both molecular and functional perspectives.

Materials and methods

Differential expression analysis of CDH13 in HCC

Data collection and processing

To evaluate the differential expression of CDH13 in HCC, publicly available RNA-seq and microarray datasets containing both HCC and non-HCC liver tissue samples were retrieved (Table 1). Inclusion criteria: (1) datasets involving human HCC tissue samples; (2) comparison between HCC and non-HCC liver tissues; (3) at least 3 samples per group. Exclusion criteria: (1) insufficient sample size; (2) CDH13 expression data unavailable; (3) metastatic or recurrent HCC samples. For cross-platform integration, we implemented a multi-step data harmonization workflow. First, raw expression data from each platform were individually preprocessed: RNA-seq data were processed using DESeq2 normalization followed by variance stabilizing transformation, while microarray data underwent background correction, quantile normalization, and probe-to-gene symbol annotation using platform-specific annotation packages. To address the heterogeneity in sample sizes across studies (ranging from 6–371 samples per dataset), we employed weighted meta-analysis approaches where each study's contribution was proportional to its sample size and variance. For datasets with varying pathological conditions (including different tumor grades, stages, and etiologies), we performed subgroup analyses and sensitivity analyses to ensure that the observed CDH13 expression patterns were robust across different clinical contexts. mRNA data were normalized and log2(x + 1) transformed. Datasets sharing the same Gene Expression Platform (GPL) platform were merged and batch effects removed. To achieve this, the "sva" R package [16], particularly the ComBat method [17], was used to adjust for batch effects, ensuring the integration of data from different platforms and experiments while minimizing technical variability. ComBat corrects for systematic differences across batches, improving data comparability. Principal component analysis (PCA) was performed before and after batch correction to visually confirm successful removal

Table 1 High-throughput sequencing datasets

Study	N_{HCC}	$N_{non\text{-}HCC\ liver}$
E_MTAB_4171	15	15
E_MTAB_8887	23	17
GPL10553	4	4
GPL10558	523	403
GPL10687	268	268
GPL10999	3	3
GPL11154	245	246
GPL13369	88	48
GPL13667	338	342
GPL14550	47	40
GPL14951	93	18
GPL15433	21	21
GPL16043	25	25
GPL16699	5	5
GPL16791	209	114
GPL17077	3	6
GPL17586	101	89
GPL18451	8	8
GPL18461	35	34
GPL18573	215	213
GPL20115	12	12
GPL20301	48	42
GPL21047	10	10
GPL23126	3	3
GPL24676	406	135
GPL3921	225	220
GPL4133	18	9
GPL5175	48	49
GPL5474	96	96
GPL570	844	528
GPL571	96	131
GPL6244	83	83
GPL6480	83	82
GPL8973	100	100
GPL6947	104	97
GPL9052	60	67
GPL9115	4	4
GPL96	5	5
ICGC_LIRI_JP	240	197
TCGA_GTEx_HCC	371	276
Hepatocellular carcinoma		

Basic information about the high-throughput sequencing datasets included in this study

of platform-specific effects while preserving biological variability. Hierarchical clustering analysis further validated that samples clustered by disease status rather than by study or platform origin. The R package "meta" (v4.18-2) was used to compute SMDs for 15,379 genes, quantifying expression differences between HCC and non-HCC tissues.

Differential gene screening

Genes were considered differentially expressed if: (1) detected in ≥ 3 studies; (2) 95% Confidence Interval (CI) of SMD did not include zero. A total of 9,296 upregulated genes (SMD > 0) and 6083 downregulated genes (SMD < 0) were identified.

Co-expression gene analysis

Spearman correlation analysis was used to identify CDH13 co-expressed genes (CEGs). Positively co-expressed genes (POS-CEGs) were defined as $R > 0.3$ and $P < 0.05$; Negatively co-expressed genes (NEG-CEGs) as $R < -0.3$ and $P < 0.05$. Final inclusion required consistent co-expression across ≥ 12 datasets.

Functional and pathway enrichment analysis

Intersection genes between Differentially expressed genes (DEGs) and CEGs were subjected to enrichment analysis using the clusterProfiler package. Pairwise similarity of enriched terms was computed using the Jaccard index and clustered with the hclust function, visualized by ggplot2 (v3.4.4). Enrichment networks were plotted using ggplot2, igraph, and ggraph. WGCNA was used to identify CDH13-related modules, and GSVA was performed using The Cancer Genome Atlas (TCGA) HCC expression profiles.WGCNA [18] is a method that clusters genes based on co-expression patterns, helping to identify gene modules linked to traits or diseases. GSVA [19] is used to estimate variation in gene set enrichment across samples, providing insights into the biological pathways activated in different samples. These approaches together helped identify the key biological processes associated with CDH13 in HCC [20].

Prognostic analysis

Prognostic data were obtained from TCGA. Univariate Cox regression assessed the impact of CDH13 and clinical variables on prognosis. Clinical entries marked "Unknown", "unreport", "Tx", "Nx", and "Mx" were excluded. Kaplan–Meier analysis evaluated the relationship between CDH13 expression and survival.

IHC of internal cohort samples

A total of 952 samples were collected: 361 HCC and 361 control samples from the First Affiliated Hospital of Guangxi Medical University, and 115 HCC and 115 controls from Yulin Red Cross Hospital. IHC was performed using CDH13 polyclonal antibody (P55290, Proteintech™, 1:2000). Sections were incubated, stained, dehydrated, and mounted under standard protocols. Staining was scored on a 0–12 scale based on % positive cells (see Table S1). Two pathologists independently scored IHC results. Cohen's kappa ($\kappa = 0.89$, $P < 0.001$) indicated strong interobserver agreement. For diagnostic performance analysis, the continuous IHC scores (0–12) were used rather than binary classification (positive/negative). Receiver operating characteristic (ROC) curve analysis was performed to evaluate the discriminatory ability of CDH13 expression in distinguishing HCC from non-HCC tissues. The AUC was calculated to quantify diagnostic accuracy. An optimal cutoff value was determined using the Youden index (sensitivity + specificity-1), which maximizes both sensitivity and specificity. Samples with scores above the cutoff were classified as CDH13-high, while those below were classified as CDH13-low. This intensity-based approach provides more refined diagnostic information compared to simple binary classification, as it captures the full spectrum of CDH13 expression levels across samples.Informed consent was obtained, and ethics approval was granted (2024-S503-01; 2024 Ethics No.8).

Proteomic data analysis

Protein expression data from the Proteomic Data Commons (https://pdc.cancer.gov/pdc/) were analyzed, including 165 HCC and 165 control tissues. Tandem mass spectrometry (MS/MS) data were processed via standard pipelines including QC, peptide identification, and protein quantification. Expression values were log2-transformed and normalized. Wilcoxon tests assessed statistical significance ($P < 0.05$).

Spatial transcriptomics of CDH13 in HCC

Spatial transcriptomics analysis used dataset GSE245908 (sample GSM7850822, GSM7850823). Data were processed in R using Seurat with SCTransform normalization. SpatialDimPlot displayed spatial distribution and CDH13 expression. Cell types were defined using canonical HCC gene markers [21–23].

CDH13 expression and CRISPR knockout in HCC cell lines

CDH13 expression and CRISPR knockout effects were obtained from the DepMap database. The CERES algorithm calculated dependency scores across HCC cell lines. Negative scores indicated growth suppression after CDH13 knockout, suggesting essentiality for proliferation. The CERES algorithm works by modeling the relationship between gene expression and growth inhibition

to calculate dependency scores. It uses a regression model that correlates the gene expression profile with the growth phenotypes of cell lines in response to genetic perturbations. A negative score indicates that the gene is essential for cell proliferation, meaning its knockout significantly reduces the growth of the cells, as observed for CDH13 in this study [24]. All cell line–based datasets in the DepMap resource undergo rigorous quality control (QC) procedures before data release. Cell line identity is confirmed through short tandem repeat (STR) profiling, and routine mycoplasma contamination testing is performed to ensure culture purity. Lineage verification, mutation status, and transcriptomic consistency are cross-validated with public reference datasets such as Cancer Cell Line Encyclopedia (CCLE) to prevent cell line misidentification or cross-contamination. In addition, DepMap applies standardized data normalization and batch-effect correction to minimize technical variability and ensure reproducibility and comparability across experimental replicates and cell line panels. These integrated QC steps guarantee the reliability and biological validity of the CDH13 dependency data used in this study [25].

scRNA-seq analysis of CDH13 in HCC

scRNA-seq data from GSE149614 were analyzed using Seurat. Seurat is a widely used tool for analyzing single-cell RNA-seq data, enabling preprocessing, clustering, and visualization of gene expression data. In this study, Seurat [26, 27] was used to perform QC, removing genes expressed in fewer than 3 cells and cells with fewer than 50 expressed genes. Cells with more than 200 genes and less than 25% mitochondrial content were retained to ensure high-quality data for downstream analysis. Seurat was then used for PCA and t-distributed stochastic neighbor embedding (t-SNE) clustering, which revealed cellular heterogeneity. Marker genes were applied to define specific cell types. CellChat, monocle, and scMetabolism were applied for communication, pseudotime, and metabolic pathway analysis.

ChIP-seq analysis of transcription factors

To identify potential transcription factors regulating CDH13 expression, we first performed co-expression analysis to identify genes significantly co-expressed with CDH13 (Pearson correlation coefficient $R > 0.3$, $P < 0.05$). These CEGs were used as input for transcription factor prediction using epigenetic Landscape In Silico deletion Analysis (LISA, http://lisa.cistrome.org/). LISA [28] is a computational method that integrates thousands of ChIP-seq profiles and chromatin accessibility data to predict transcription factors whose binding sites are enriched in the regulatory regions of query genes. The algorithm models the regulatory potential of transcription factors by calculating the statistical significance of their binding enrichment near the transcriptional start sites of CEGs, thereby identifying master regulators of the input gene set. Based on LISA predictions, FOXA1 was identified as a top-ranked transcription factor potentially regulating CDH13. To validate this prediction, ChIP-seq data for FOXA1 were obtained from Cistrome Data Browser (Cistrome DB) [29], focusing on HUH7 cell line. CDH13 promoter/enhancer regions were analyzed for FOXA1 binding sites to confirm the direct regulatory relationship.

Immune and immunotherapy correlation analysis

CDH13 expression data from HiPlot were used to analyze 15 immunotherapy cohorts (anti–PD-1/PD-L1, CAR-T, anti–MAGE-A3, etc.). Expression was compared between responders (R) and non-responders (NR) using t-test or Wilcoxon test. Kaplan–Meier curves and log-rank tests assessed prognostic impact. CIBERSORT analysis, based on TCGA Transcripts per million (TPM) RNA-seq data, inferred immune cell proportions and correlations with CDH13.

Chemotherapy sensitivity and molecular docking

Spearman correlation analysis was performed to assess the associations between CDH13 expression and drug sensitivity, measured by AUC or half-maximal inhibitory concentration (IC50), using data from Cancer Therapeutics Response Portal (CTRP, https://portals.broadinstitute.org/ctrp/), Profiling Relative Inhibition Simultaneously in Mixtures (PRISM, https://depmap.org/portal/prism/), and Genomics of Drug Sensitivity in Cancer (GDSC, https://www.cancerrxgene.org/) databases. Drug selection was performed through a multi-step prioritization process. First, drugs with available sensitivity data across at least 50% of HCC cell lines were retained to ensure statistical robustness. Second, Spearman correlation coefficients and corresponding p-values were calculated for each drug. Drugs were then ranked based on the absolute value of the correlation coefficient ($|R|$) combined with statistical significance ($P < 0.05$). To identify the most promising candidates, we selected the top 30 drugs showing the strongest correlations (either positive or negative) with CDH13 expression, prioritized by p-value in cases where correlation coefficients were similar. This approach ensured that the selected drugs had both statistically significant and biologically meaningful associations with CDH13 expression levels. Molecular docking simulations were conducted using CB-based Docking (CB-DOCK, http://cao.labshare.cn/cb-dock/) to evaluate the binding affinity between CDH13 and candidate compounds. The three-dimensional structure

of CDH13 was obtained from the Alphafold (ID: AF-P55290-5-F1-model_v6), and the chemical structure of docetaxel was retrieved from PubChem (CID: 148124). Binding affinity was quantified using the Vina score, with values < −4 kcal/mol indicating strong binding interactions.

Assessing the impact of CDH13 on phenotypic traits

The AstraZeneca phenome-wide association study (PheWAS) Portal (https://www.azphewas.com/) was utilized to investigate potential associations between CDH13 and diverse phenotypic traits. This platform employs a PheWAS approach, integrating exome sequencing (ES) data from large-scale cohorts such as the UK Biobank. The methodology involves gene-based collapsing analyses of rare protein-coding variants to identify significant gene-phenotype associations. This analysis was performed to evaluate whether CDH13 influences clinically relevant phenotypic traits, providing insights into its potential broader physiological roles and implications for drug discovery.

Statistical analysis

Wilcoxon tests compared CDH13 expression levels. Fixed-effects models were used when $I^2 < 50\%$; otherwise, random-effects models were applied. ROC and Summary receiver operating characteristic (sROC) curves were generated using pROC and STATA 18.0, respectively. AUC quantified diagnostic performance. Publication bias was evaluated using Begg's test ($P > 0.05$ indicating no bias).

Results

Overview of analysis workflow

The overall workflow of this study is illustrated in Fig. 1.

High expression of cdh13 at mrna and protein levels in HCC

CDH13 was significantly upregulated at both mRNA and protein levels in HCC. We integrated RNA-seq and microarray data from 40 public platforms (Fig. 2), including 4,000 non-HCC controls and 5,145 HCC samples. CDH13 mRNA expression was elevated in HCC with an SMD of 1.17 (95% CI 0.854–1.49). Begg's test indicated no publication bias ($P > 0.05$; Fig. 3A), and funnel plots showed no heterogeneity (Fig. 3B). Correlation analysis confirmed consistent results (Fig. 3C). CDH13 overexpression was also associated with poor overall survival (HR = 2.06, 95% CI 1.19–3.59, $P < 0.05$) (Figure S1A, B).

Protein-level expression was validated by IHC using 361 HCC and 361 non-HCC samples from the First Affiliated Hospital of Guangxi Medical University, and 115 HCC and 115 non-HCC samples from Yulin Red Cross Hospital. IHC showed no CDH13 staining in non-HCC tissues, while moderate cytoplasmic and partial membranous staining was observed in HCC tissues (Fig. 4A). Additional validation using 165 paired HCC and non-HCC samples from the Proteomic Data Commons showed consistent overexpression with an SMD of 2.48 (95% CI 0.717–4.24; Fig. 4B). Funnel plots showed no heterogeneity (Fig. 4C), and correlation analysis supported the reliability (Fig. 4D).

CDH13 demonstrated high diagnostic performance in all three datasets: AUC = 0.935 (95% CI 0.907–0.963) in the Proteomic Data Commons, 0.975 (95% CI 0.959–0.991) in Guangxi cohort, and 0.954 (95% CI 0.924–0.985) in Yulin cohort (Figure S2A). mRNA-level diagnostic analysis yielded a pooled sensitivity of 0.83 (95% CI 0.77–0.88), specificity of 0.77 (95% CI 0.71–0.82), and AUC of 0.87 (95% CI 0.84–0.90) (Figure S2B).

Spatial transcriptomics, CRISPR, and scRNA-seq analyses

Spatial transcriptomics analysis (Fig. 5A) showed significant CDH13 upregulation in tumor regions (Fig. 5B, C). Cell abundance mapping (Fig. 5D) revealed that tumor cell scores were elevated in CDH13-rich areas and spatially associated with endothelial cells, whereas B, T, and NKT cells did not overlap.Spatial transcriptomic mapping of an independent HCC tissue section showed that CDH13 expression was primarily enriched in tumor regions and overlapped with areas of high endothelial scores, further supporting the CDH13–endothelial association (Fig. 5E).

CDH13 was highly expressed in HCC cell lines such as SNU182, SNU739, and HUH7 (Fig. 6A). CRISPR knockout significantly inhibited the proliferation of these cells (Fig. 6B). scRNA-seq QC indicated high-quality data (Fig. 7A). PCA showed sample continuity and no batch effects (Fig. 7B); variable genes revealed cell heterogeneity (Fig. 7C). CNV confirmed tumor cell identity (Fig. 7D). Major cell clusters included endothelial, fibroblast, hepatocyte, myeloid, and T/NK cells (Fig. 7E), from normal, tumor, PVTT, and lymph tissues (Fig. 7F), stratified by HBV/HCV status (Fig. 7G). CDH13 was expressed in hepatocytes, endothelial, tumor, and HBV + regions (Fig. 7H, I); IHC confirmed moderate positivity in tumor cells and strong positivity in vascular endothelial structures (Fig. 7J).

Pseudotime analysis (Figure S3A) showed clear trajectory phases with endothelial cells at the terminal stage and CDH13 highly expressed during late differentiation. Cell identity markers validated clustering accuracy (Figure S3B).

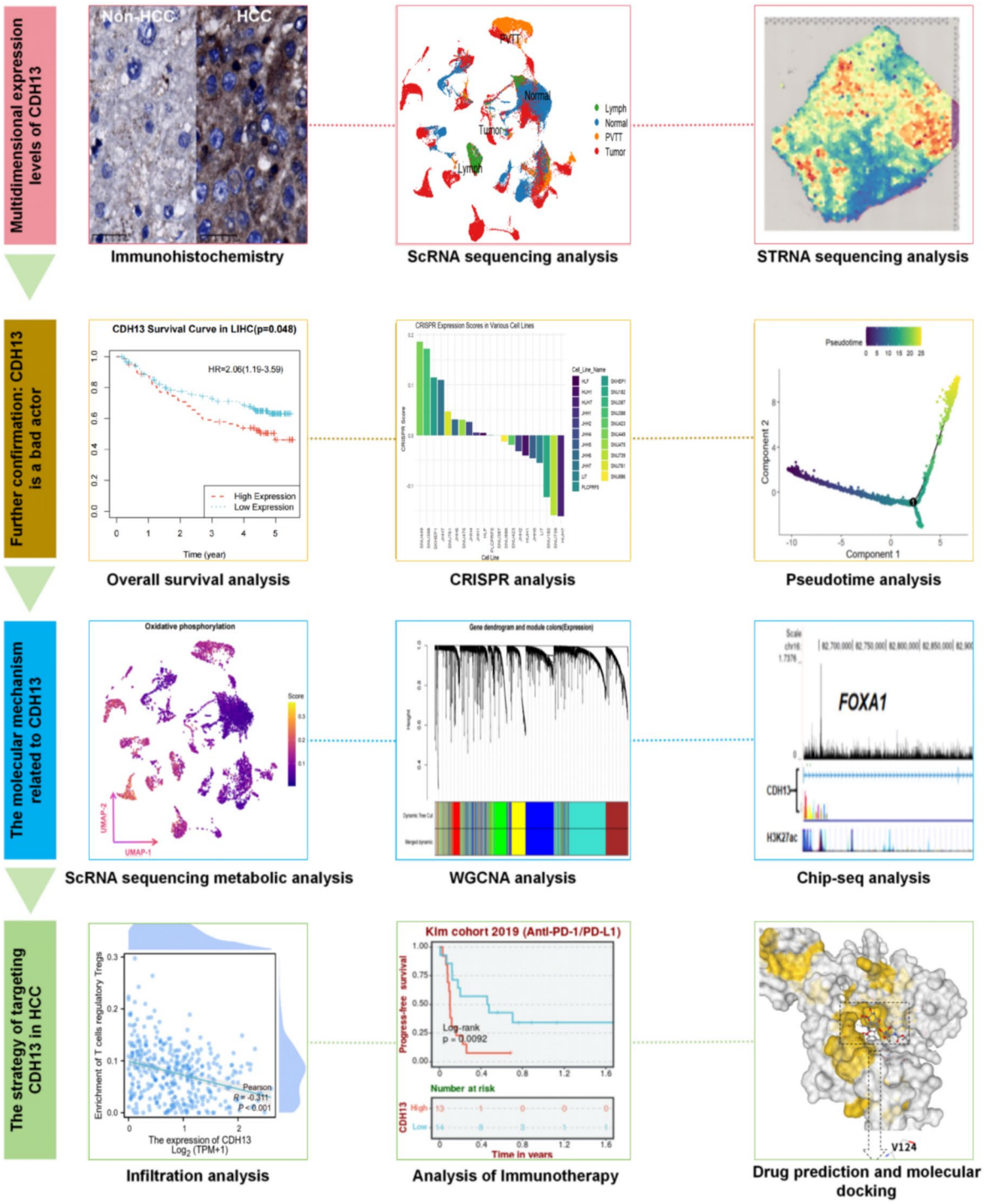

Fig. 1 Analysis Workflow. Schematic representation of the analytical workflow for the study

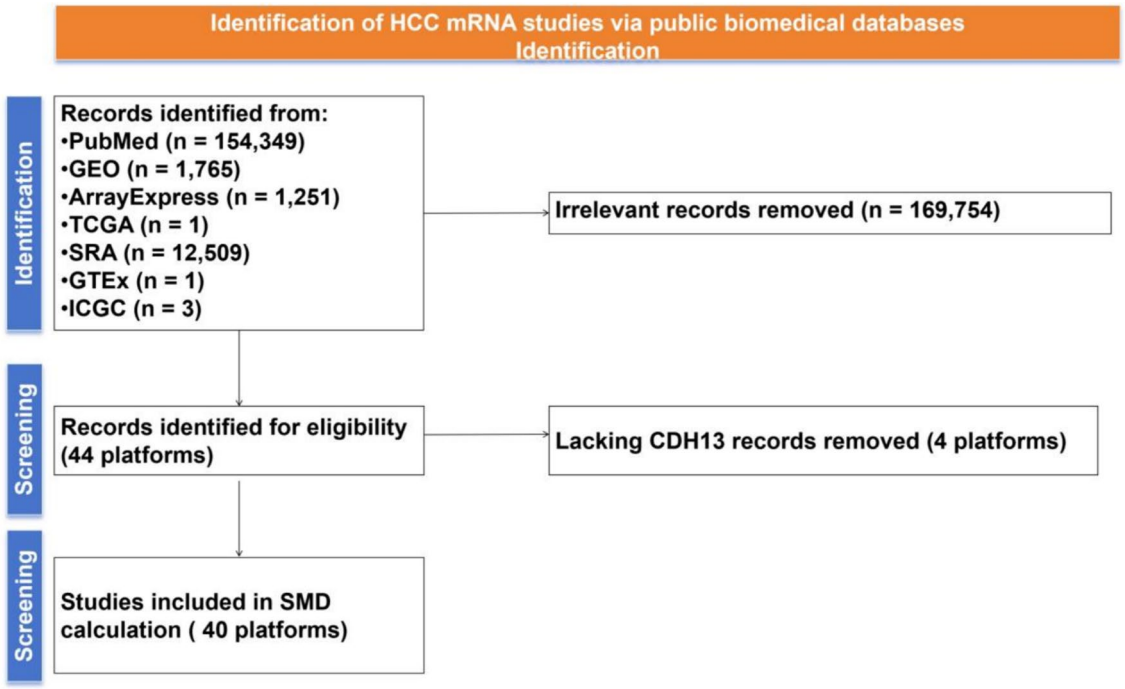

Fig. 2 Data Selection Flowchart. Flowchart illustrating the identification of HCC mRNA studies from public biomedical databases

Cellular communication and MIF pathway analysis

CellChat analysis revealed extensive interactions among fibroblasts, endothelial, hepatocytes, myeloid, and T/NK cells (Fig. 8A). Signal input/output activity varied among cell types (Fig. 8B). MIF was the dominant communication pathway, with ligand-receptor pairs (MIF-CD74-CD44, MIF-CD74-CXCR4) highly specific (Fig. 8C). Communication matrices and role analysis showed hepatocytes and endothelial cells acted as signal senders (Fig. 8D, E), with differential pathway contributions across cell types (Fig. 8F, G). Network analysis confirmed complex regulatory roles with MIF as a central axis (Fig. 8H).

Metabolic and molecular mechanisms of CDH13 in HCC

UMAP of scMetabolism revealed metabolic heterogeneity across cell types, with high scores for pyrimidine metabolism, oxidative phosphorylation, and glutathione metabolism in endothelial cells (Figure S4A, B). WGCNA and GSVA related to CDH13 in HCC revealed its critical role in the TME (Figure S5). The gene clustering dendrogram (Figure S5A) categorized genes into multiple modules based on expression patterns, with colored bands marking module classifications, illustrating the modular distribution of gene expression. Network parameter validation (Figure S5B) demonstrated that soft threshold selection was optimized through scale-free network fitting ($R^2 > 0.8$) and average connectivity, determining the optimal parameters for network construction. The module-module correlation heatmap (Figure S5C) displayed the strength of expression associations between modules, suggesting potential synergistic interactions. The scatter plot of module membership versus gene significance (Figure S5D) indicated significant correlations between module genes and HCC phenotypes, highlighting the biological significance of core genes. The module-phenotype association matrix (Figure S5E) showed a positive correlation between modules and the Q4 phenotype (correlation coefficient 0.74, $P < 0.05$), successfully identifying core modules. The GSVA pathway enrichment waterfall plot (Figure S5F), based on TCGA expression profile data, ranked enriched pathways of module genes by P-value, with pathway enrichment represented by bar height (blue for low-expression group, red for high-expression group). Metabolic pathways, such as mannose-type O-glycan biosynthesis and oxidative phosphorylation, were significantly enriched in the high-expression group ($P < 0.05$), suggesting that high expression may activate these pathways, with endothelial cell metabolic reprogramming being particularly prominent, consistent with prior metabolic analysis results, validating the critical role of module genes in endothelial cell metabolic reprogramming. The scatter plot of CDH13 correlation with HCC oncogenic features (Figure S5G) showed positive correlations with angiogenesis ($R = 0.56$, $P < 0.05$), invasion ($R = 0.36$, $P < 0.05$), and apoptosis ($R = 0.21$, $P < 0.05$).

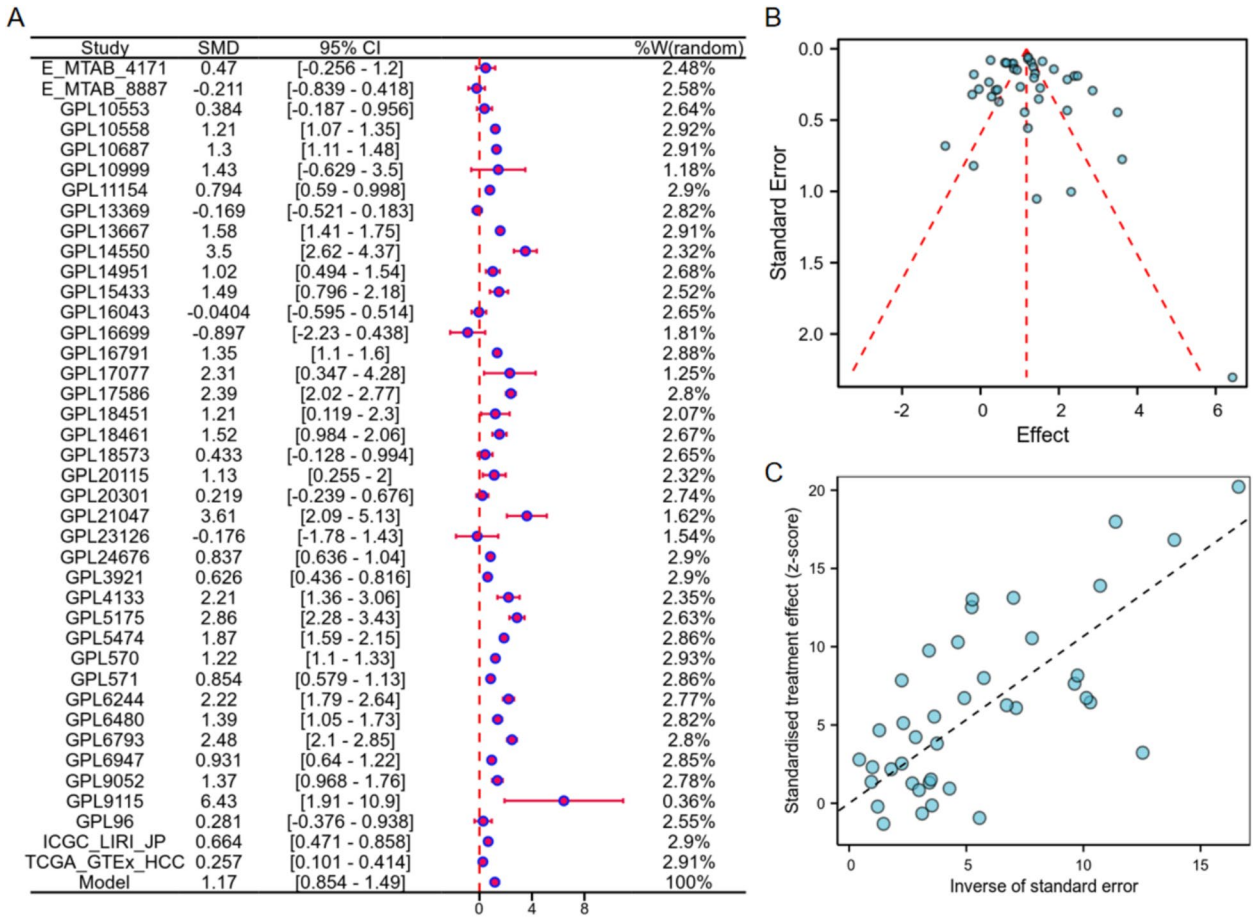

Fig. 3 CDH13 mRNA Overexpression in HCC. Analysis of CDH13 mRNA expression based on 4000 non-HCC controls and 5,145 HCC patient samples. **A** Standardized mean difference (SMD) plot for CDH13 mRNA expression. **B** Funnel plot assessing publication bias and heterogeneity. **C** Correlation plot demonstrating result consistency

Further functional enrichment analysis of CDH13-related gene sets elucidated its molecular mechanisms (Figure S6). Intersection analysis of CDH13 POS-CEG (Figure S6A) revealed that the HCC high-expression SMD > 0 gene set (6,802 unique genes) intersected with CDH13 POS-CEG to yield 2,494 genes, of which 115 were unique to CDH13 POS-CEG, forming the core associated gene pool. Functional enrichment analysis of positively correlated genes (Figure S6B) indicated significant enrichment in pathways such as oocyte meiosis, cell cycle, cellular senescence, tubulin binding, DNA catalytic activity, ATP-dependent DNA activity, organelle fission, nuclear division, chromosome segregation, chromosome centromeric region, chromosomal region, and condensed chromosome (P adj range 2.0e-07–5.0e-08, gene count 50–150), revealing the role of CDH13 POS-CEG in key HCC biological processes. The enriched pathway association network for positively correlated genes (Figure S6C) demonstrated synergy among cell cycle, chromosome segregation, nuclear division, and organelle fission pathways, with node attributes consistent with Figure S6B (P adj color gradient, gene count size). Intersection analysis of CDH13 negatively correlated genes (CDH13 NEG-CEG) (Figure S6D) showed that the HCC low-expression SMD < 0 gene set (5843 unique genes) intersected with CDH13 NEG-CEG to yield 240 genes, of which 4 were unique to CDH13 NEG-CEG, identifying negatively correlated core genes. Functional enrichment analysis of negatively correlated genes (Figure S6E) indicated significant enrichment in pathways such as fatty acid degradation, tryptophan metabolism, carboxylic acid catabolism, small molecule catabolism, α-amino acid metabolism, paired donor redox, molecular oxygen redox, monooxygenase activity, steroid hydroxylase activity, retinol metabolism, lipoprotein particles, plasma lipoprotein particles, and protein-lipid complexes (gene count 10–30), elucidating the role of CDH13 NEG-CEG in metabolic regulation. The enriched pathway association network for negatively correlated genes (Figure S6F) illustrated collaborative patterns among fatty acid

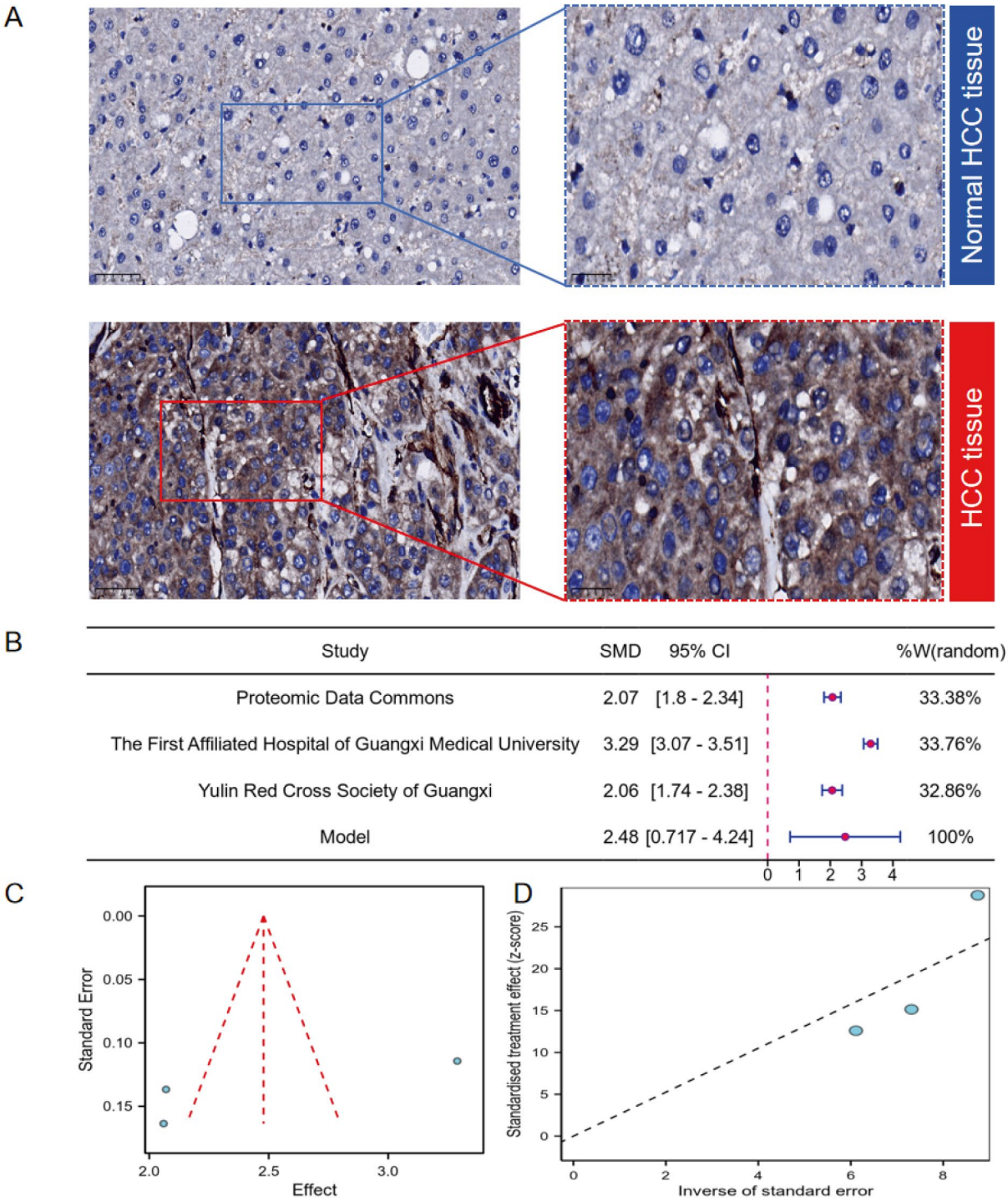

Fig. 4 CDH13 Protein Overexpression in HCC. Analysis of CDH13 protein expression using multi-center data, including 165 non-HCC controls and 165 HCC samples from Proteomic Data Commons, 361 non-HCC controls and 361 HCC samples from the First Affiliated Hospital of Guangxi Medical University, and 115 non-HCC controls and 115 HCC samples from Yulin Red Cross Hospital. **A** Immunohistochemistry (IHC) images of CDH13 in non-HCC and HCC tissues. **B** Standardized mean difference (SMD) plot for CDH13 protein expression across three independent cohorts. Each study's contribution is shown with its SMD, 95% confidence interval (CI), and weight percentage in the random-effects model (%W(random)). The overall pooled effect (Model) demonstrates significant CDH13 overexpression in HCC tissues. **C** Funnel plot evaluating heterogeneity. **D** Correlation plot confirming result consistency

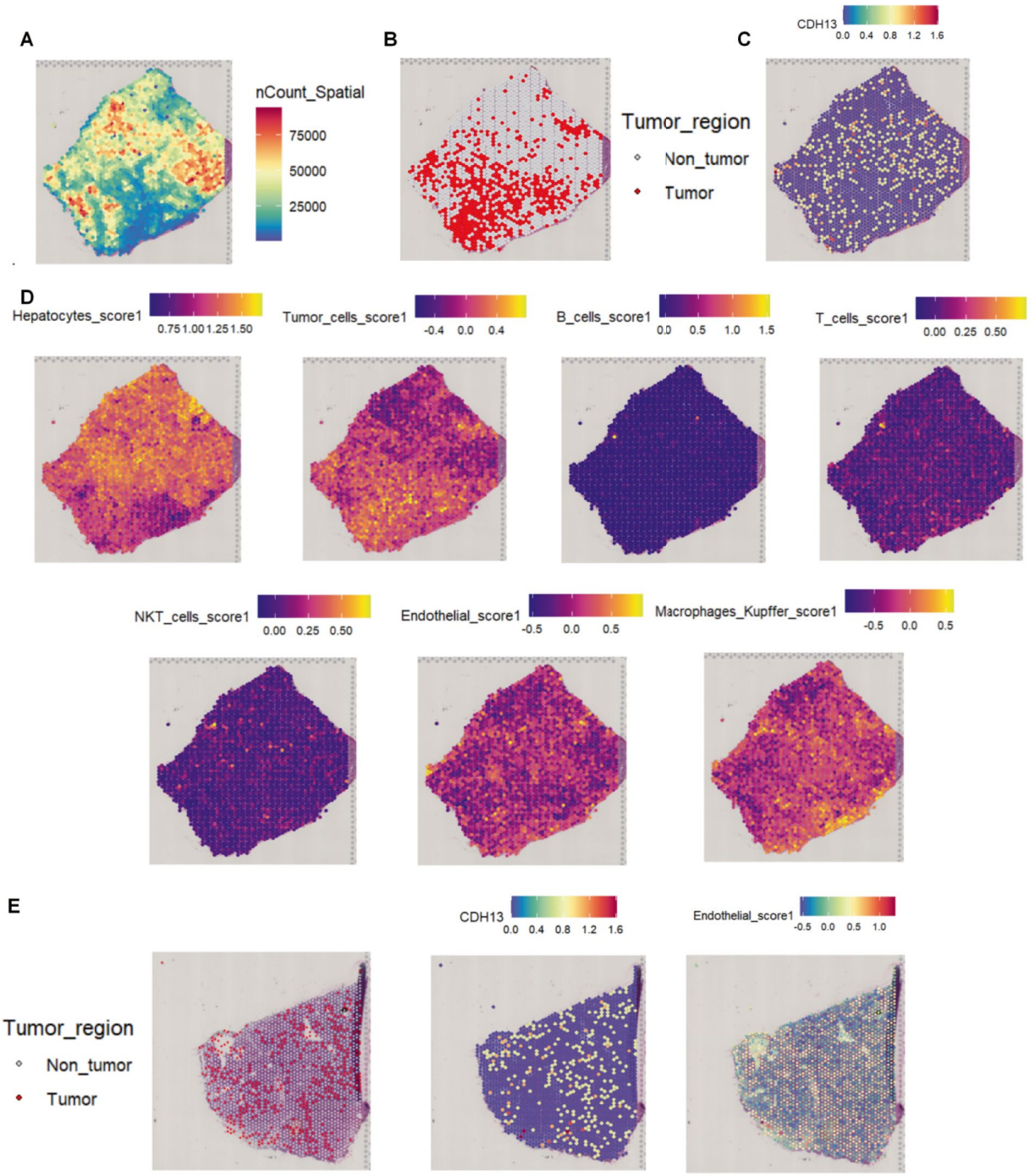

Fig. 5 Spatial Transcriptomics of CDH13 in HCC. Spatial transcriptomic analysis of one HCC tissue section revealing CDH13 overexpression in tumor regions. **A** Spatial distribution of sequencing data (nCount_Spatial). **B** Delineation of tumor and adjacent non-tumor regions. **C** Spatial distribution of CDH13 gene expression (high in tumor regions). **D** Spatial abundance distribution of various cell types. **E** Spatial distribution of CDH13 expression and endothelial features in HCC tissue

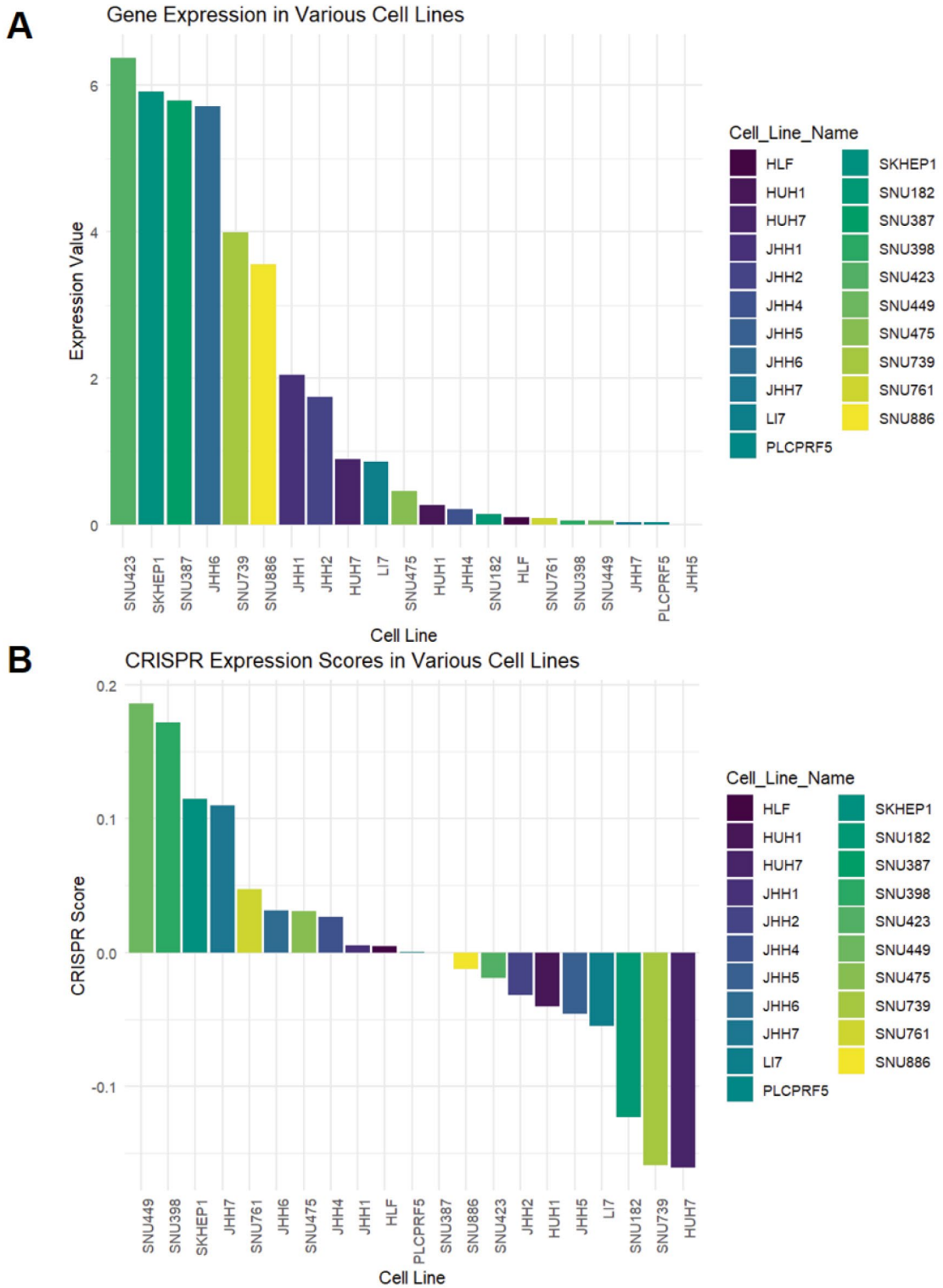

Fig. 6 Effect of CDH13 Knockout in HCC Cells. Impact of knocking out highly expressed CDH13 in HCC cell lines. **A** CDH13 gene expression levels across different HCC cell lines. **B** Expression scores post-CRISPR knockout of CDH13 in HCC cell lines. CRISPR Score (also known as CRISPR dependency score or gene effect score) represents the impact of gene knockout on cell viability and proliferation. This score is derived from large-scale CRISPR-Cas9 screening data (such as from the DepMap project)

degradation, small molecule catabolism, carboxylic acid catabolism, and lipoprotein particle pathways, with node attributes consistent with Figure S6E (P adj color gradient, similarity 0.4–1.0).

FOXA1-mediated transcriptional regulation of CDH13

Candidate TFs were screened using HCC DEGs (SMD > 0) and integrated TF prediction databases. FOXA1 and RELA were selected for validation (Fig. 9A). ScRNA-seq and spatial transcriptomics revealed heterogeneous spatial patterns for FOXA1 and RELA (Fig. 9B, C). Both were overexpressed in HCC at the mRNA level (Table 2). ChIP-seq in HUH7 cells confirmed specific binding of FOXA1, but not RELA, to CDH13 promoter/enhancer regions, overlapping with active histone marks and regulatory elements (Fig. 9D).

CDH13 and immune microenvironment/immunotherapy prediction

Based on the TCGA database, a systematic analysis was conducted to investigate the role of CDH13 in regulating the HCC immune microenvironment and predicting immunotherapy response. The CIBERSORT algorithm revealed that CDH13 expression was associated with 22 immune cell types, showing negative correlations with regulatory T cells (Tregs, $R = -0.311$, $P < 0.05$), γδ T cells ($R = -0.206$, $P < 0.05$), and follicular helper T cells ($R = -0.167$, $P < 0.05$) (Figure S7A). Moreover, high CDH13 expression reduced the enrichment scores of these three T cell subtypes (Figure S7B). Immune microenvironment scoring analysis indicated that CDH13 expression was positively correlated with stromal score (StromaScore, $R = 0.400$, $P < 0.05$) and comprehensive score (ESTIMATEScore, $R = 0.192$, $P < 0.05$) (Figure S7C), with the ESTIMATE and stromal scores significantly higher in the high CDH13 expression group compared to the low expression group (Figure S7D). Scatter plots demonstrated statistically significant correlations between CDH13 expression and immune cell and stromal scores (Figure S7E). Immunotherapy response prediction was validated in three independent cohorts: in the Gao 2018 cohort (anti-PD-1/CTLA-4 therapy), high CDH13 expression was significantly associated with immunotherapy resistance, evidenced by distinct expression differences between responders and non-responders, with an ROC curve AUC of 0.745. In the Kim 2019 cohort (anti-PD-1/PD-L1 therapy), high CDH13 expression was linked to immunotherapy insensitivity, with an AUC of 0.795, and the high expression group exhibited significantly worse overall survival compared to the low expression group, indicating poorer prognosis. In the iMvigor210 cohort (anti-PD-L1 therapy), high CDH13 expression was similarly associated with treatment insensitivity, with an AUC of 0.586 (Figure S7F).

Docetaxel targeting and phenotype association of CDH13

Molecular docking showed high binding affinity (binding score:−7.6 kcal/mol) (Fig. 10A).Drug sensitivity analysis revealed that CDH13 expression was negatively correlated with docetaxel IC_{50} values, indicating that higher CDH13 expression may be associated with increased docetaxel sensitivity (Fig. 10B).PheWAS indicated no significant association of CDH13 with infection, immunity, or organ-specific phenotypes, suggesting low toxicity risk for CDH13-targeted therapies (Fig. 10C).

Discussion

This study integrates multi-omics data to systematically elucidate CDH13's expression profile, molecular mechanisms, and complex interactions with the tumor microenvironment in HCC, providing strong evidence for its potential as a diagnostic biomarker and therapeutic target. A key strength is the large-scale cohort, comprising 952 tissue samples (361 HCC and 361 non-HCC controls from the First Affiliated Hospital of Guangxi Medical University, and 115 HCC and 115 non-HCC controls from Yulin Red Cross Hospital), alongside multi-omics data from 40 platforms (4000 non-HCC controls and 5145 HCC samples). This extensive analysis enhances result robustness and representativeness, addressing limitations of prior studies with smaller cohorts, such as a peripheral blood mononuclear cell study of 157 HCC patients [11] That study reported CDH13 promoter hypermethylation linked to mRNA downregulation and poor prognosis but lacked tumor tissue analysis. This study employs RNA-seq, proteomics,

(See figure on next page.)

Fig. 7 Single-Cell Transcriptomics of CDH13 in HCC. Single-cell transcriptomic analysis based on principal component analysis (PC1-12) showing CDH13 overexpression in malignant tumor cells. **A** Quality control plot displaying gene expression and mitochondrial RNA proportions. **B** PCA plot illustrating sample distribution. **C** Heatmap of top differentially expressed genes and variance contributions for the first four principal components. **D** Chromatin accessibility and gene expression heatmap comparing tumor and normal samples. **E** t-SNE clustering plot by cell type. **F** t-SNE clustering plot by tissue origin (tumor, normal, etc.). **G** t-SNE plot showing cell distribution by hepatitis virus infection status (HBV, HCV, etc.). **H** t-SNE plot of CDH13 expression distribution. **I** Boxplot of CDH13 expression across cell types/tissue regions with statistical differences. **J** IHC images of HCC tissues showing CDH13 protein localization

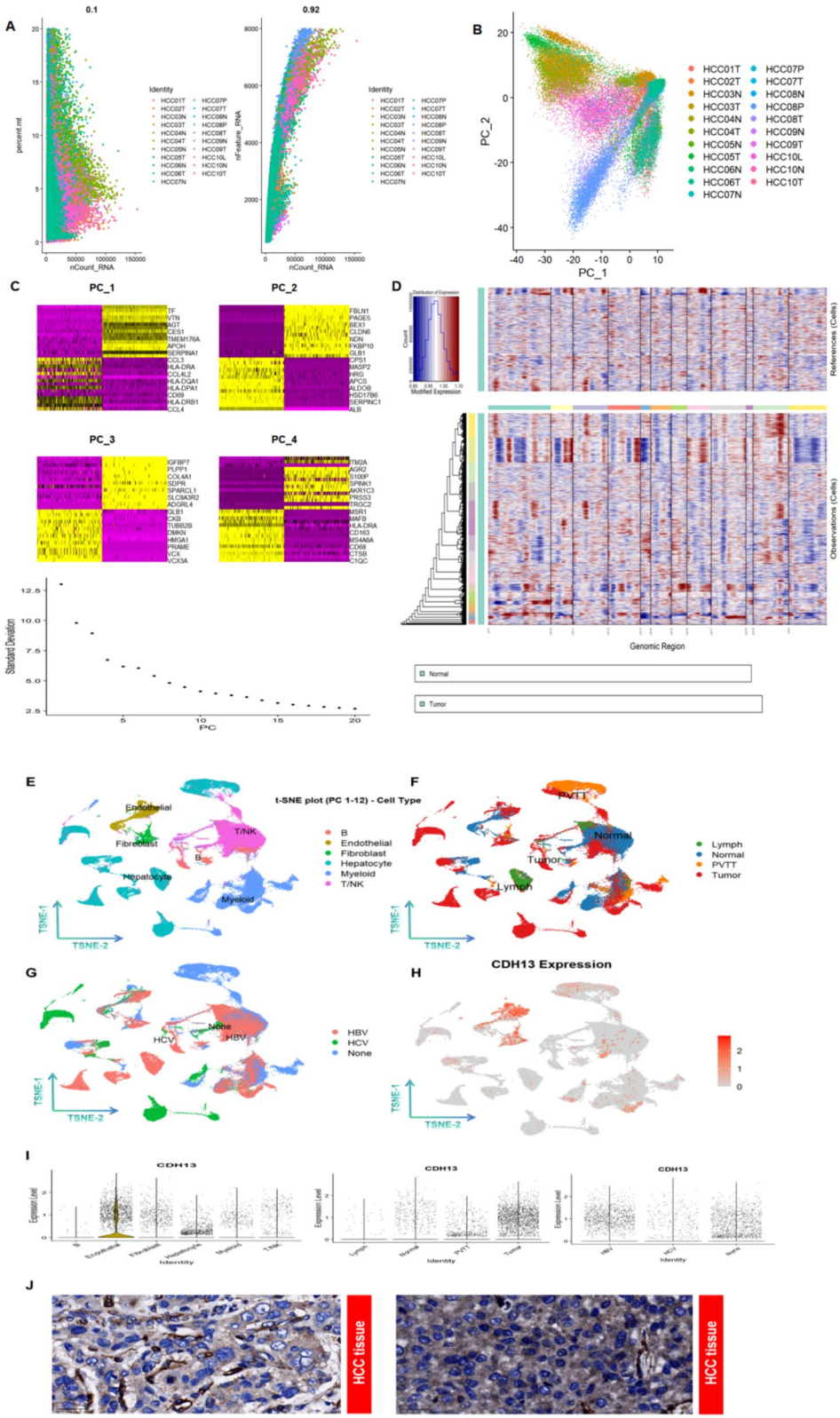

Fig. 7 (See legend on previous page.)

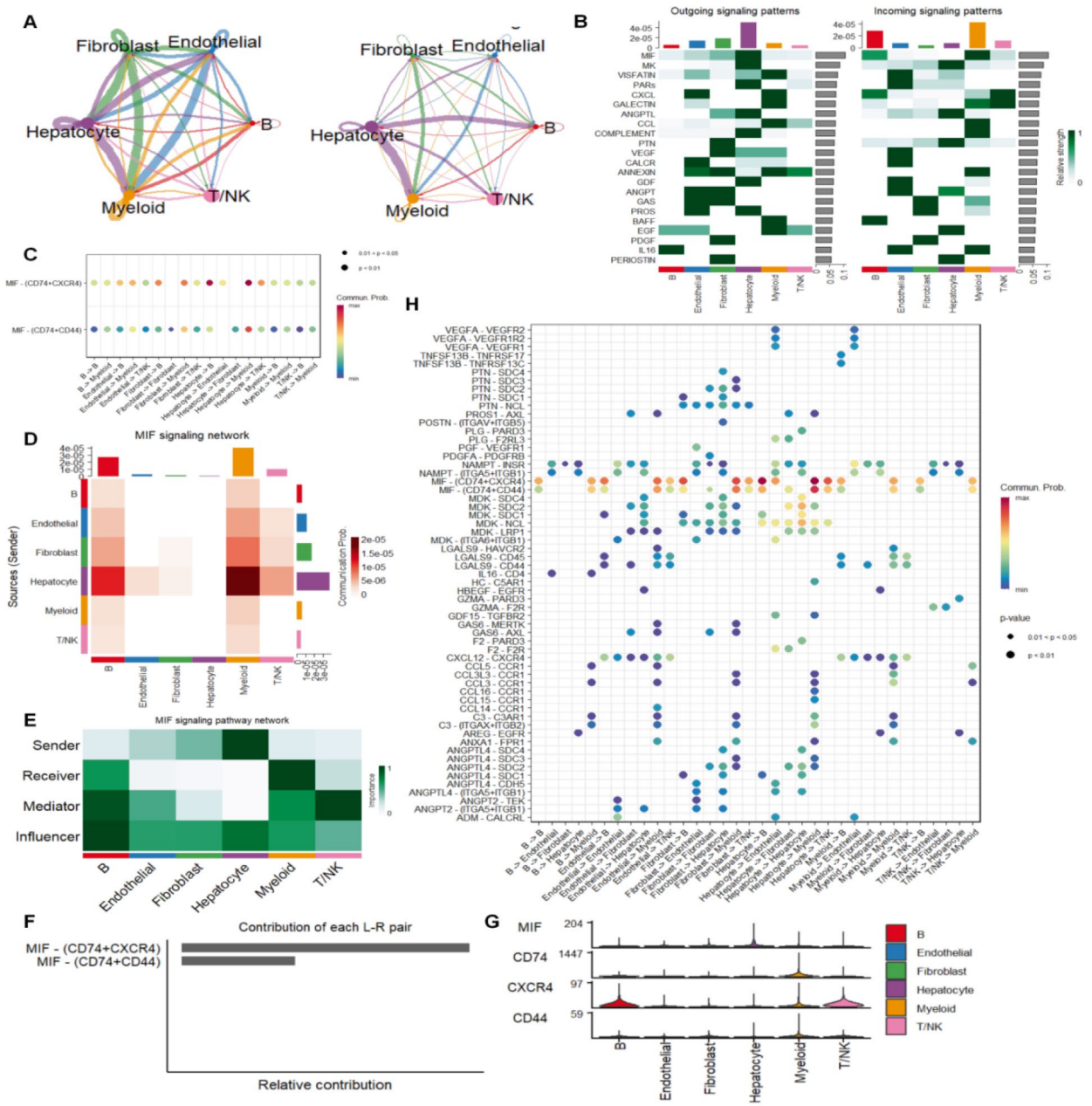

Fig. 8 Cell Communication and MIF Pathway Analysis in HCC Microenvironment. Analysis of cell communication and MIF pathway interactions in the HCC microenvironment. **A** Cell communication network showing signal interactions among fibroblasts, endothelial cells, etc. (left–right comparison of modes). **B** Heatmap of outgoing and incoming signaling pathway activities. **C** Dot plot of MIF pathway ligand-receptor expression (e.g., MIF-CD74-CD44) across cell types. **D** MIF pathway communication matrix (top, showing sender-receiver strength) and network (bottom, illustrating signal transmission). **E** Heatmap of MIF pathway cell roles (Sender, Receiver, etc.). **F** Relative contribution of MIF pathway ligand-receptor pairs. **G** Violin plot of MIF pathway molecule expression (MIF, CD74, etc.) across cell types. **H** Multi-pathway molecular interaction network integrating molecular and cell type associations

immunohistochemistry, scRNA-seq, and spatial transcriptomics to comprehensively investigate CDH13 expression patterns, signaling pathway regulation, and microenvironmental roles in HCC tumor tissues and endothelial cells, revealing its multidimensional functions in HCC progression. The following discussion analyzes CDH13's molecular mechanisms, microenvironmental interactions, and clinical translational potential,

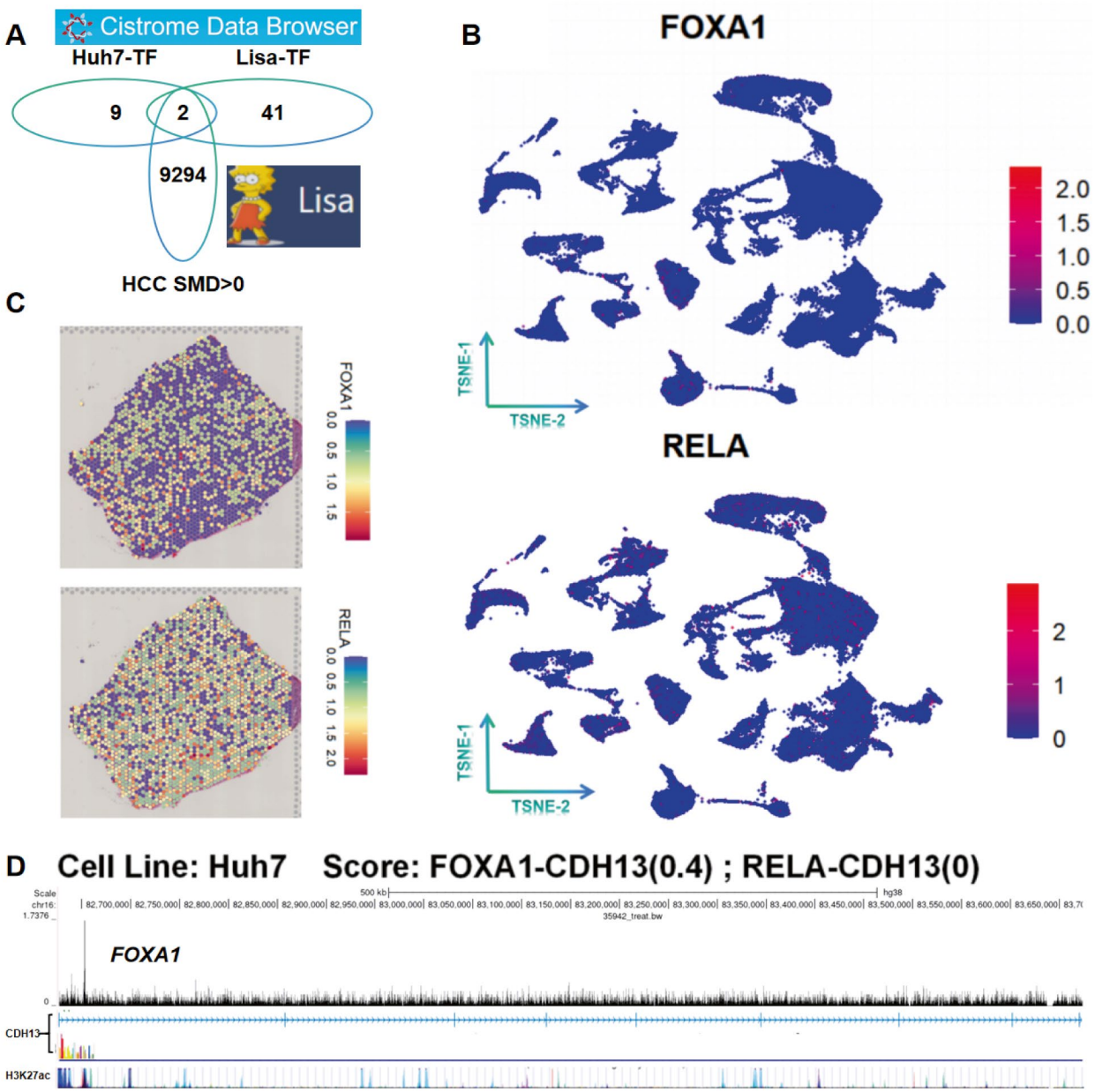

Fig. 9 FOXA1-CDH13 Transcriptional Regulation in HCC. Investigation of the FOXA1-CDH13 transcriptional regulation axis in HCC. **A** Venn diagram of transcription factor database intersection (Huh7-TF, Lisa-TF, Cistrome DB) with HCC high-expression genes (SMD > 0) for candidate selection. **B** Single-cell expression plots of FOXA1 and RELA. **C** Spatial transcriptomic analysis showing spatial expression distributions of FOXA1 (0.0–1.5) and RELA (0.0–2.0) in HCC tissue sections. **D** ChIP-seq results showing FOXA1-CDH13 binding score (0.4) and RELA-CDH13 binding score (0), validating FOXA1's regulatory role

Table 2 Overexpression of FOXA1 and RELA mRNA in HCC

symbol	SMD	lower.CI	upper.CI	I2	p
FOXA1	0.250810298679635	0.116288960040006	0.385331637319211	0.802843651899592	0.000257900847727907
RELA	0.198936946939391	0.153752303447257	0.244121590431526	0.816002589936093	6.17595631773513e−18

Standardized mean difference (SMD) and confidence intervals for FOXA1 and RELA mRNA expression in HCC

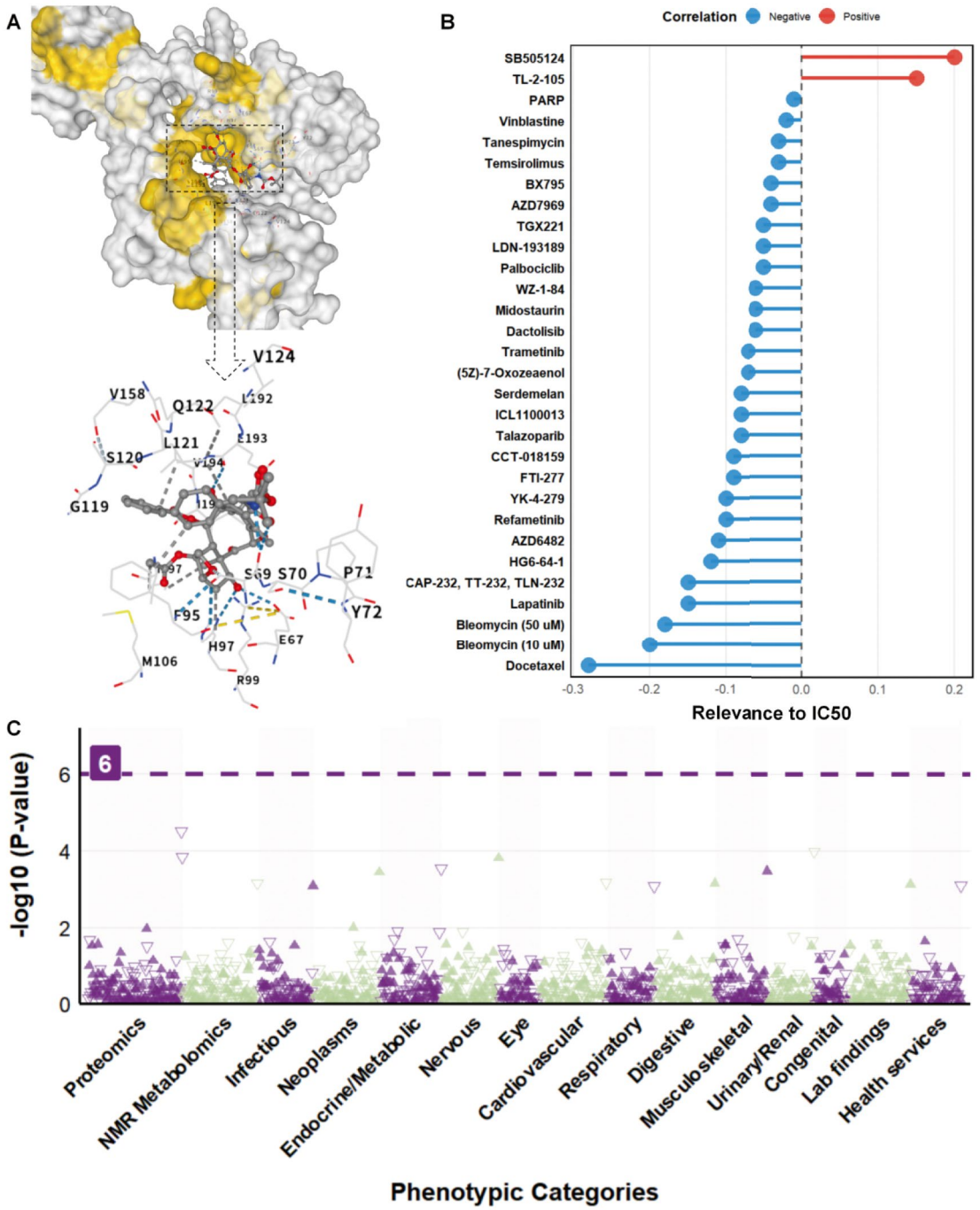

Fig. 10 Docetaxel as a CDH13-Targeted Drug Validation and safety assessment of Docetaxel as a CDH13-targeted drug. **A** Molecular docking analysis: 3D protein structure and 2D interaction diagrams showing Docetaxel-CDH13 binding affinity. **B** Forest plot of CDH13 expression correlations with anti-tumor drug sensitivities, highlighting Docetaxel ($P < 0.001$). **C** Manhattan plot of CDH13 full-phenotype toxicity analysis, assessing association strengths (–log10 P) across physiological and pathological phenotypes

integrating potential mechanistic changes to elucidate its biological significance in HCC.

Multi-omics analysis confirmed distinct CDH13 expression characteristics in HCC, particularly its high expression in tumor regions and endothelial cells, contrasting with prior peripheral blood mononuclear cell methylation studies. Immunohistochemistry revealed CDH13 expression predominantly in HCC tumor cell cytoplasm and partial membrane, with minimal staining in non-HCC tissues, suggesting CDH13 may regulate HCC's malignant phenotype through specific expression. ChIP-Seq analysis identified direct binding of transcription factor FOXA1 to CDH13 promoter and enhancer regions, indicating a FOXA1-CDH13 transcriptional regulatory axis that likely enhances tumor cell proliferation and invasion by activating CDH13 transcription. As a key regulator of hepatocyte differentiation and HCC progression, FOXA1 may cooperate with histone acetyltransferases (e.g., p300/CBP) [30] to open the CDH13 locus chromatin structure, increasing transcriptional activity. This activation may upregulate VEGFA expression, amplifying CDH13-mediated angiogenesis [31], contributing to HCC's hypervascular phenotype. Moreover, CDH13's GPI-anchored property positions it as a cell membrane signaling molecule, potentially interacting with lipoproteins (e.g., LDL), growth factors (e.g., VEGF, FGF), or extracellular matrix components to activate downstream pathways, such as PI3K/AKT [32], MAPK/ERK [33], and Wnt/β-catenin [34]. These pathway activations may trigger mechanistic changes: PI3K/AKT, via phosphorylation of mTOR and BAD [35, 36], inhibits apoptosis and promotes metabolic reprogramming, enhancing HCC cell adaptation to nutrient-deficient environments; MAPK/ERK, by upregulating Cyclin D1 and c-Myc [37], accelerates G1/S cell cycle transition, promoting tumor proliferation; Wnt/β-catenin, by activating EMT-related genes (e.g., Snail, Twist) [38], enhances HCC invasion and metastasis. WGCNA and GSVA showed CDH13-related genes enriched in cell cycle, chromosome segregation, and metabolic pathways (e.g., oxidative phosphorylation, pyrimidine metabolism), suggesting CDH13 drives HCC rapid proliferation and metabolic adaptability. Oxidative phosphorylation activation may provide energy for tumor cells [39], supporting high proliferation demands, while enhanced pyrimidine metabolism may supply nucleotides for DNA and RNA synthesis [40], accelerating HCC malignant progression.

Endothelial cells are central to HCC's tumor microenvironment, driving angiogenesis, nutrient supply, and immune cell recruitment. Recent studies have emphasized the importance of endothelial cell metabolic reprogramming in HCC progression, indicating that endothelial cells undergo significant metabolic shifts that promote tumor growth and angiogenesis. For example, Fidgetin-like 1 (FIGNL1) was shown to regulate the extracellular matrix-receptor interaction pathway, modulating HCC formation, which may suggest that endothelial cells' metabolic and ECM-related pathways are critical for tumor vascularization and progression in HCC [41, 42]. Spatial transcriptomics revealed high CDH13 expression in tumor regions, with clear spatial co-localization with endothelial cells, suggesting it shapes an immunosuppressive microenvironment by regulating cell adhesion, signal transduction, and metabolic pathways. CDH13's spatial distribution correlates with endothelial cells (high PECAM1, VWF expression), tumor cells, and immune cells. ScRNA-seq confirmed CDH13 expression patterns in hepatocytes, endothelial cells, and HBV-infected regions, with pseudotime analysis indicating high expression in late differentiation stages, implying a key role in HCC late-stage progression, particularly in endothelial cell metabolic reprogramming. GSVA showed CDH13-related genes enriched in oxidative phosphorylation and pyrimidine metabolism pathways, consistent with endothelial cells' high energy and nucleic acid synthesis demands in the tumor microenvironment [43], suggesting CDH13 enhances endothelial cell metabolic activity, supporting tumor vascular network formation and HCC rapid proliferation. Additionally, CDH13's interaction with the MIF pathway highlights its role in immune microenvironment remodeling. The MIF pathway, via CD74 and CD44 signaling, promotes immunosuppressive cell recruitment (e.g., Tregs, MDSCs) [44]. This study found CDH13 expression negatively correlated with Tregs and γδT cells, suggesting it may enhance HCC immune escape by downregulating immune effector cell activity. This aligns with previous findings suggesting that immune checkpoint-related immune cell dynamics play a key role in regulating immune responses and prognosis in HCC. For instance, mitochondrial lipid metabolism genes have been identified as diagnostic and prognostic biomarkers for HCC, linking lipid metabolism with immune modulation in the tumor microenvironment. Additionally, immune cell dynamics in the HCC microenvironment have been shown to influence the efficacy of immunotherapies, further supporting CDH13's potential in immunotherapy stratification [45, 46].This immunosuppression may occur via CDH13-mediated TGF-β or VEGF pathways, with TGF-β inducing Treg differentiation [47] and VEGF upregulating PD-L1 expression [48], reducing anti-PD-1/PD-L1 therapy efficacy. CIBERSORT analysis showed high CDH13 expression positively correlated with stromal and comprehensive scores, suggesting it enhances stromal cell (e.g., fibroblast) and endothelial cell activity, constructing a pro-tumor microenvironment.

CRISPR experiments demonstrated CDH13 knockout significantly inhibited proliferation in HCC cell lines (e.g., SNU182, HUH7), highlighting its therapeutic target potential. Molecular docking analysis confirmed docetaxel's high binding affinity to CDH13, indicating targeted therapy feasibility. CDH13 knockout may exert anti-tumor effects by regulating cell cycle and apoptosis pathways (e.g., p53, Bcl-2, Caspase) [49]. For instance, CDH13 knockout may downregulate Cyclin D1 or upregulate p21, arresting the cell cycle at G1/S, or induce apoptosis via Caspase-3/7 activation. These mechanistic changes may synergize with CDH13's role in PI3K/AKT or MAPK/ERK pathways, amplifying anti-tumor effects. This study also found that CDH13 expression correlated with chemotherapy drug sensitivity through molecular docking and drug IC50 prediction analyses, particularly for docetaxel, suggesting that high CDH13 expression may be associated with altered drug binding characteristics and cellular drug response. However, CDH13's role across HCC subtypes and etiologies requires further investigation. HBV-related HCC may exhibit unique mechanisms due to viral regulation (e.g., HBx-mediated signaling), while HCV or non-alcoholic fatty liver disease-related HCC may involve miRNA (e.g., miR-21, miR-155) [50] or lncRNA-mediated post-transcriptional regulation. The large-scale cohort data provide robust support for these findings, but future studies should include more non-HBV-related HCC samples, integrate in vivo models (e.g., mouse xenografts, patient-derived organoids) to validate CDH13's functional mechanisms, and explore its combination with immunotherapies (e.g., anti-PD-1/PD-L1, CAR-T). Additionally, CDH13's potential as a non-invasive biomarker requires validation of its expression in serum, exosomes, or circulating tumor cells to improve HCC early diagnosis sensitivity and specificity. Developing CDH13-targeted strategies, such as antibody-drug conjugates or nanoparticle delivery systems, may open new avenues for HCC treatment.

In summary, this study, through large-scale cohort data and multi-omics analysis, elucidates CDH13's expression characteristics and molecular mechanisms mediated via FOXA1 transcriptional regulation, PI3K/AKT, MAPK/ERK, MIF, and metabolic pathways in HCC. CDH13's strong correlation with endothelial cells and its role in immunosuppressive microenvironments highlight its critical functions in HCC angiogenesis and immune escape. Docetaxel binding and CRISPR knockout results further support its therapeutic target potential. However, the lack of in vivo validation using xenograft models represents a limitation of this study, and future investigations should prioritize validating CDH13's functional role in tumor growth and angiogenesis through animal models. Additionally, functional validation of the relationship between CDH13 expression and docetaxel sensitivity through cell viability assays and in vivo efficacy studies is warranted to clarify whether CDH13 directly modulates the therapeutic response to docetaxel. Furthermore, while our bioinformatics analyses suggest CDH13's involvement in TGF-β/VEGF-mediated immune escape pathways, protein-level validations including Western blot for TGF-β and ELISA for VEGF are lacking, which limits the mechanistic understanding of CDH13-mediated immunosuppression. Future research should focus on CDH13's functional heterogeneity across HCC subtypes, dynamic regulation of mechanistic changes, and synergistic effects with immunotherapy to advance its clinical translation in HCC precision diagnosis and treatment.

Abbreviations

HCC	Hepatocellular carcinoma
CDH13	Cadherin 13
scRNA-seq	Single-cell RNA sequencing
IHC	Immunohistochemistry
CRISPR/Cas9	Clustered regularly interspaced short palindromic repeats/CRISPR-associated protein 9
ChIP-seq	Chromatin immunoprecipitation sequencing
WGCNA	Weighted gene co-expression network analysis
GSVA	Gene set variation analysis
SMD	Standardized mean difference
HR	Hazard ratio
HBV	Hepatitis B virus
MIF	Macrophage migration inhibitory factor
FOXA1	Forkhead box A1
Tregs	Regulatory T cells
AUC	Area under the curve
GPI	Glycosylphosphatidylinositol
PBMCs	Peripheral blood mononuclear cells
HCV	Hepatitis C virus
VEGF	Vascular endothelial growth factor
PCA	Principal component analysis
CI	Confidence interval
POS-CEGs	Positively co-expressed genes
NEG-CEGs	Negatively co-expressed genes
DEGs	Differentially expressed genes
CEGs	Co-expressed genes
TCGA	The Cancer Genome Atlas
RNA-seq	RNA sequencing
MS/MS	Tandem mass spectrometry
STR	Short tandem repeat
CCLE	Cancer Cell Line Encyclopedia
t-SNE	T-distributed stochastic neighbor embedding
LISA	Epigenetic Landscape In Silico deletion Analysis
TPM	Transcripts per million
CTRP	Cancer Therapeutics Response Portal
PRISM	Profiling Relative Inhibition Simultaneously in Mixtures
GDSC	Genomics of Drug Sensitivity in Cancer
PheWAS	Phenome-wide association study
ROC	Receiver operating characteristic
sROC	Summary receiver operating characteristic
QC	Quality control
GPL	Gene Expression Platform
IC50	Half-maximal inhibitory concentration
ES	Exome sequencing
Cistrome DB	Cistrome Data Browser
CB-DOCK	CB-based Docking
PD-1	Programmed death protein 1
PD-L1	Programmed deathligand 1
FIGNL1	Fidgetin-like 1

Supplementary Information

The online version contains supplementary material available at https://doi.org/10.1186/s40001-025-03667-0.

Supplementary Material 1. Figure S1: Prognostic analysis of CDH13 in HCC. **A** Disease-specific survival curve of CDH13 in LIHC. **B** Overall survival curve of CDH13 in LIHC. Figure S2: Diagnostic Performance of CDH13 in HCC. Receiver Operating Characteristic (ROC) and Summary ROC (SROC) analyses demonstrating the diagnostic efficacy of CDH13 at protein and mRNA levels. **A** ROC curve for protein-level expression. **B** SROC curve for mRNA-level expression. Figure S3: Pseudotime Analysis of HCC Cell Differentiation. Single-cell pseudotime analysis revealing HCC cell differentiation trajectories and CDH13 expression dynamics. **A** Pseudotime trajectory plots (from left to right, top to bottom): differentiation trajectories by state, cell type, and tissue site; pseudotime value-colored trajectory; CDH13 expression trajectory; line plot of CDH13 relative expression across cell types over pseudotime. **B** Histogram of marker gene expression, showing expression levels (color) and proportions (dot size) of characteristic genes (e.g., CD19, MS4A1) across cell types (T/NK, myeloid, etc.). Figure S4: Single-Cell Metabolic Pathway Analysis in HCC. Single-cell metabolic pathway analysis in HCC. **A** UMAP plot showing activity distribution of metabolic pathways (e.g., pyrimidine metabolism, glycosphingolipid metabolism) across cell subtypes, with color gradients indicating pathway scores. **B** Bar plot of enriched metabolic pathways in endothelial cells, comparing tumor and normal states. Figure S5: WGCNA and GSVA Analysis of CDH13 in HCC. Weighted Gene Co-expression Network Analysis (WGCNA) and Gene Set Variation Analysis (GSVA) of CDH13 in HCC. **A** Gene clustering dendrogram with module assignments indicated by colored bands. **B** Network parameter validation: left, scale-free network fit; right, mean connectivity for soft threshold selection. **C** Module-module correlation heatmap showing expression association strengths. **D** Scatter plot of module membership versus gene significance for HCC phenotypes. **E** Module-phenotype association matrix displaying correlation coefficients and P-values for modules and HCC phenotypes (Q1-Q4). **F** GSVA pathway enrichment waterfall plot based on TCGA data, ranking enriched pathways by P-value. **G** Scatter plots of CDH13 correlations with HCC oncogenic features (e.g., angiogenesis, invasion). Figure S6: Functional Enrichment Analysis of CDH13-Related Gene Sets in HCC. Functional enrichment analysis of CDH13-related gene sets in HCC. **A** Venn diagram of CDH13 positive co-expression genes (POS-CEG) intersecting with HCC high-expression genes (SMD > 0). **B** Tree diagram of enriched functions for POS-CEG. **C** Weighted network of enriched pathways for POS-CEG, showing inter-pathway associations. **D** Venn diagram of CDH13 negative co-expression genes (NEG-CEG) intersecting with HCC low-expression genes (SMD < 0). **E** Tree diagram of enriched functions for NEG-CEG. **F** Weighted network of enriched pathways for NEG-CEG (e.g., lipid metabolism, fatty acid degradation). *POS-CEG: R > 0.3, P < 0.05; NEG-CEG: R < -0.3, P < 0.05; SMD > 0: HCC high-expression genes; SMD < 0: HCC low-expression genes. Figure S7: CDH13 and Immune Microenvironment in HCC. Analysis of CDH13's association with the HCC immune microenvironment and immunotherapy response based on TCGA data. **A** Correlation analysis of CDH13 expression with 22 immune cell types using CIBERSORT, showing R and P-values. **B** Histogram of enrichment scores for key immune cells (Tregs, γδ T cells, etc.) in CDH13 high- and low-expression groups. **C** Correlation analysis of CDH13 expression with stroma, immune, and ESTIMATE scores. **D** Histogram comparing immune microenvironment scores in CDH13 high- and low-expression groups. **E** Scatter plots validating CIBERSORT immune score correlations. **F** Immunotherapy response prediction using ROC curves and survival analyses in independent cohorts (Gao 2018, Kim 2019, iMvigor210). *P < 0.05, **P < 0.01, ***P < 0.0001. Table S1: IHC staining scoring criteria

Author contributions

Ke-Jun Wu, Jian-Di Li, Lu Zhang, and Qi Li conducted sequencing data and gene chip data screening, computation, and visualization analysis. They also performed single-cell sequencing analysis, spatial transcriptomics analysis, immune infiltration analysis, and evaluated immunohistochemical results. Additionally, they carried out gene pathway operations and contributed to drafting the initial manuscript. Di-Yuan Qin, Shi-De Li, and Ji-Feng He provided guidance on computational pathology and molecular functional visualization operations. Li-Hua Yang, Rong-Quan He, and Jian-Jun Li provided guidance on statistical analysis and manuscript revisions. Dong-Ming Li, Yi-Wu Dang, Ming-Jie Li, and Han He designed the INHOUSE validation experiments, performed immunohistochemical procedures, and guided the evaluation of the results. Gang Chen and Xiao-Bo Jiang designed the entire project, supervised all experiments and computations, and completed the manuscript.

Funding

National Natural Science Foundation of China(NSFC82460783, NSFC82160762);Innovation Project of Guangxi Graduate Education (JGY2023068);Guangxi Medical University "Four New" Project(SX202403);China Undergraduate Innovation and Entrepreneurship Training Program(S202310598177); Future Academic Star of Guangxi Medical University (WLXSZX23110).

Data availability

No datasets were generated or analysed during the current study.

Declarations

Ethics approval and consent to participate

Approval was obtained from the ethics committee of The First Affiliated Hospital of Guangxi Medical University. The procedures used in this study adhere to the tenets of the Declaration of Helsinki. Informed consent was obtained from all individual participants included in the study.

Consent for publication

Consent for publication was obtained for every individual person's data included in the study.

Competing interests

The authors declare no competing interests.

Author details

[1]Department of Pathology, The First Affiliated Hospital of Guangxi Medical University, 6 Shuang yong RD, Guangxi Zhuang Autonomous Region, Nanning 530021, People's Republic of China. [2]Department of Medical Oncology, The First Affiliated Hospital of Guangxi Medical University, 6 Shuangyong RD, Guangxi Zhuang Autonomous Region, Nanning 530021, People's Republic of China. [3]Department of Computer Science and Technology, School of Computer and Electronic Information, Guangxi University, 100 Daxuedong RD, Guangxi Zhuang Autonomous Region, Nanning 530 004, People's Republic of China. [4]Department of General Surgery, The Second Affiliated Hospital of Guangxi Medical University, Guangxi Zhuang Autonomous Region, Nanning, People's Republic of China. [5]Department of General Practice, The First Affiliated Hospital of Guangxi Medical University, 6 Shuang yong RD, Guangxi Zhuang Autonomous Region, Nanning 530021, People's Republic of China.

Received: 11 July 2025 Accepted: 5 December 2025
Published online: 12 December 2025

References

1. Xiang Z, Li J, Xu Y, Xu C, Zheng S, Chen J, et al. Cell differentiation-related signaling pathways in hepatocellular carcinoma metastasis. Cancer Lett. 2025;627:217846. https://doi.org/10.1016/j.canlet.2025.217846.
2. He Y, Liu D, Ling A, Han Z, Cui J, Cheng J, et al. Inhibition of Wnt/beta-catenin increases anti-tumor activity by synergizing with sorafenib in hepatocellular carcinoma. Cell Death Dis. 2025;16(1):466. https://doi.org/10.1038/s41419-025-07789-5.
3. Friehmann T, Abu Mohsen Y, Schlesinger Y, Ghantous L, Gamaev L, Landau Zenilman C, et al. The oncogenic microRNA miR-222 promotes human LINE-1 retrotransposition. RNA Biol. 2025;22(1):1–15. https://doi.org/10.1080/15476286.2025.2511318.
4. Situ Y, Deng L, Huang Z, Jiang X, Zhao L, Zhang J, et al. CDH2 and CDH13 as potential prognostic and therapeutic targets for adrenocortical carcinoma. Cancer Biol Ther. 2024;25(1):2428469. https://doi.org/10.1080/15384047.2024.2428469.

5. Sysoeva V, Semina E, Klimovich P, Kulebyakin K, Dzreyan V, Sotskaya E, et al. T-cadherin modulates adipogenic differentiation in mesenchymal stem cells: insights into ligand interactions. Front Cell Dev Biol. 2024;12:1446363. https://doi.org/10.3389/fcell.2024.1446363.
6. Dasen B, Pigeot S, Born GM, Verrier S, Rivero O, Dittrich PS, et al. T-cadherin is a novel regulator of pericyte function during angiogenesis. Am J Physiol Cell Physiol. 2023;324(4):C821–36. https://doi.org/10.1152/ajpcell.00326.2022.
7. Kyriakakis E, Maslova K, Frachet A, Ferri N, Contini A, Pfaff D, et al. Crosstalk between EGFR and T-cadherin: EGFR activation promotes T-cadherin localization to intercellular contacts. Cell Signal. 2013;25(5):1044–53. https://doi.org/10.1016/j.cellsig.2013.02.001.
8. Popov VS, Brodsky IB, Balatskaya MN, Balatskiy AV, Ozhimalov ID, Kulebyakina MA, et al. T-Cadherin Deficiency Is Associated with Increased Blood Pressure after Physical Activity. Int J Mol Sci. 2023. https://doi.org/10.3390/ijms241814204.
9. Wen Y, Ma L, Liu Y, Xiong H, Shi D. Decoding the enigmatic role of T-cadherin in tumor angiogenesis. Front Immunol. 2025;16:1564130. https://doi.org/10.3389/fimmu.2025.1564130.
10. Baranova I, Samec M, Dvorska D, Stastny I, Janikova K, Kasubova I, et al. Droplet digital PCR analysis of CDH13 methylation status in Slovak women with invasive ductal breast cancer. Sci Rep. 2024;14(1):14700. https://doi.org/10.1038/s41598-024-65580-6.
11. Yuan XD, Wang JW, Fang Y, Qian Y, Gao S, Fan YC, et al. Methylation status of the T-cadherin gene promotor in peripheral blood mononuclear cells is associated with HBV-related hepatocellular carcinoma progression. Pathol Res Pract. 2020;216(5):152914. https://doi.org/10.1016/j.prp.2020.152914.
12. Shen W, Li Z, Huang J, Zhang G, Tang Y, Fan W, et al. Development and validation of nomogram including mutations in angiogenesis-related genes as risk factors for HCC patients treated with TACE. Transl Oncol. 2025;58:102437. https://doi.org/10.1016/j.tranon.2025.102437.
13. Fu C, Liang Q, Ma L, Liu W, Guo W, Wang G. miR-29a-3p/Vegfa axis modulates high phosphate-induced vascular smooth muscle cell calcification. Ren Fail. 2025;47(1):2489712. https://doi.org/10.1080/0886022X.2025.2489712.
14. Huang LX, Qiu ZX, Wang XX, Wang ZL, Feng B. Endothelial cells expressing CPE and vWF are involved in the immunopathogenesis of primary biliary cholangitis. Sci Rep. 2025;15(1):22640. https://doi.org/10.1038/s41598-025-07311-z.
15. Cui C, Cui F, Zou Q, Zhang Z, Jia L. Progress and applications of single-cell RNA sequencing and spatial transcriptome technology in acute kidney injury research. Mol Ther Nucleic Acids. 2025;36(3):102583. https://doi.org/10.1016/j.omtn.2025.102583.
16. Chen H, Su X, Li Y, Dang C, Luo Z. Identification of metabolic reprogramming-related genes as potential diagnostic biomarkers for diabetic nephropathy based on bioinformatics. Diabetol Metab Syndr. 2024;16(1):287. https://doi.org/10.1186/s13098-024-01531-5.
17. Wakasugi N, Takano H, Abe M, Sawamoto N, Murai T, Mizuno T, et al. Harmonizing multisite data with the ComBat method for enhanced Parkinson's disease diagnosis via DAT-SPECT. Front Neurol. 2024;15:1306546. https://doi.org/10.3389/fneur.2024.1306546.
18. Zou JH, Wang HW, Long JZ, Yang XN, Yang LH, Li LJ, et al. Unveiling the diagnostic and causal role of hyperlipidemia- and lipophagy-associated genes PLAUR, IVNS1ABP, and QKI in acute myocardial infarction. Int J Cardiol. 2025;441:133635. https://doi.org/10.1016/j.ijcard.2025.133635.
19. Cai Y, Yu D, Meng J, Qiu Y, Liu J, Yao J. Multi-omics analysis and validation of autophagy-related diagnostic biomarker in osteoarthritis. Ann Med. 2025;57(1):2548045. https://doi.org/10.1080/07853890.2025.2548045.
20. Ferreira MR, Santos GA, Biagi CA, Silva Junior WA, Zambuzzi WF. GSVA score reveals molecular signatures from transcriptomes for biomaterials comparison. J Biomed Mater Res A. 2021;109(6):1004–14. https://doi.org/10.1002/jbm.a.37090.
21. Luo Y, Wang X. Integration of single-cell and bulk RNA sequencing data to identify liquid-liquid phase separation-related prognostic biomarkers in hepatocellular carcinoma. Sci Rep. 2025;15(1):36805. https://doi.org/10.1038/s41598-025-20691-6.
22. Chen S, Li Y, Hu J, Li H, Hu C, Zhao J, et al. Integrating bulk RNA-seq, scRNA-seq, and spatial transcriptomics data to identify novel post-translational modification-related molecular subtypes and therapeutic responses in hepatocellular carcinoma. Cancer Cell Int. 2025;25(1):330. https://doi.org/10.1186/s12935-025-03964-y.
23. Wang S, Wu P, Xu N, Xiao Z, Liu Y, Bian W, et al. MSR1 + macrophages passivate antitumor immunity by inducing ITM2A + CD4T exhaustion differentiation. Hepatology. 2025. https://doi.org/10.1097/HEP.0000000000001578.
24. Meyers RM, Bryan JG, McFarland JM, Weir BA, Sizemore AE, Xu H, et al. Computational correction of copy number effect improves specificity of CRISPR-Cas9 essentiality screens in cancer cells. Nat Genet. 2017;49(12):1779–84. https://doi.org/10.1038/ng.3984.
25. Sannigrahi MK, Cao AC, Rajagopalan P, Sun L, Brody RM, Raghav L, et al. A novel pipeline for prioritizing cancer type-specific therapeutic vulnerabilities using DepMap identifies PAK2 as a target in head and neck squamous cell carcinomas. Mol Oncol. 2024;18(2):336–49. https://doi.org/10.1002/1878-0261.13558.
26. Butler A, Hoffman P, Smibert P, Papalexi E, Satija R. Integrating single-cell transcriptomic data across different conditions, technologies, and species. Nat Biotechnol. 2018;36(5):411–20. https://doi.org/10.1038/nbt.4096.
27. Tan Z, Chen X, Zuo J, Fu S, Wang H, Wang J. Comprehensive analysis of scRNA-Seq and bulk RNA-Seq reveals dynamic changes in the tumor immune microenvironment of bladder cancer and establishes a prognostic model. J Transl Med. 2023;21(1):223. https://doi.org/10.1186/s12967-023-04056-z.
28. Qin Q, Fan J, Zheng R, Wan C, Mei S, Wu Q, et al. Lisa: inferring transcriptional regulators through integrative modeling of public chromatin accessibility and ChIP-seq data. Genome Biol. 2020;21(1):32. https://doi.org/10.1186/s13059-020-1934-6.
29. Taing L, Dandawate A, L'Yi S, Gehlenborg N, Brown M, Meyer CA. Cistrome data browser: integrated search, analysis and visualization of chromatin data. Nucleic Acids Res. 2024;52(D1):D61–6. https://doi.org/10.1093/nar/gkad1069.
30. Rosell M, Nevedomskaya E, Stelloo S, Nautiyal J, Poliandri A, Steel JH, et al. Complex formation and function of estrogen receptor alpha in transcription requires RIP140. Cancer Res. 2014;74(19):5469–79. https://doi.org/10.1158/0008-5472.CAN-13-3429.
31. Quan H, Ren C, Xie H, He Z, Ding H, Li J, et al. An injectable hydrogel loaded with miRNA nanocarriers promotes vessel-associated osteoclast (VAO)-mediated angiogenesis and bone regeneration in osteonecrosis of the rat femoral head. Biomaterials. 2025;320:123252. https://doi.org/10.1016/j.biomaterials.2025.123252.
32. Xi Y, Huang Y, Hu J, Wang Y, Qian Q, Tu L, et al. EIF2B5 promotes malignant progression of hepatocellular carcinoma by activating the PI3K/AKT signaling pathway through targeting RPL6. Cell Signal. 2025;132:111821. https://doi.org/10.1016/j.cellsig.2025.111821.
33. Lu G, Zhuang X, Wang C, Ge Z, Wu M, Chen M, et al. Bergenin exerts anti-cancer activity in hepatocellular carcinoma via the PI3K/Akt/mTOR and MAPK/ERK pathways. J Mol Histol. 2025;56(4):213. https://doi.org/10.1007/s10735-025-10498-0.
34. Wen W, Wang R. Consensus artificial intelligence-driven prognostic signature for predicting the prognosis of hepatocellular carcinoma: a multicenter and large-scale study. NPJ Precis Oncol. 2025;9(1):207. https://doi.org/10.1038/s41698-025-01010-8.
35. Wang Z, Xiao Y, Huang A, Zhang L, Luo H. Attenuation of brucine action on DMBA/TPA-induced skin cancer by PI3K/Akt/mTOR signaling. J Mol Histol. 2025;56(4):216. https://doi.org/10.1007/s10735-025-10524-1.
36. Sohel M. Breaking barriers; phytoestrogens in the fight against triple-negative breast cancer: a comprehensive review. Med Res Rev. 2025;45(4):1211–50. https://doi.org/10.1002/med.22107.
37. Dai P, Wang L. Targeting c-MYC has a key role in hepatocellular carcinoma therapy. Crit Rev Oncol Hematol. 2025;213:104786. https://doi.org/10.1016/j.critrevonc.2025.104786.
38. Thapa R, Gupta S, Gupta G, Bhat AA, Smriti SM, et al. Epithelial-mesenchymal transition to mitigate age-related progression in lung cancer. Ageing Res Rev. 2024. https://doi.org/10.1016/j.arr.2024.102576.
39. Zhang L, Liu T, Chen M, Gao S, Staley CA, Yang L, et al. Dual inhibition of oxidative phosphorylation and glycolysis using a hyaluronic acid nanoparticle NOX inhibitor enhanced response to radiotherapy in colorectal cancer. Biomaterials. 2025;323:123437. https://doi.org/10.1016/j.biomaterials.2025.123437.
40. Yu YZ, Xie X, Cai MP, Hong YY, Ren YZ, Kang X, et al. Identification of pyrimidine metabolism-based molecular subtypes and prognostic

signature to predict immune landscape and guide clinical treatment in prostate cancer. Ann Med. 2025;57(1):2449584. https://doi.org/10.1080/07853890.2025.2449584.
41. You S, Cheng N, Wang F, Zheng X, Wang Y, Zhao B, et al. Hsa_circ_0001687 function as a ceRNA to facilitate hepatocellular carcinoma progression via miR-140- 3p/FOXQ1 axis. Protein Peptide Lett. 2023;30(11):930–40. https://doi.org/10.2174/0109298665238824231012072118.
42. Wang J, Sun L, Liu Y, Zhang Y. FIGNL1 promotes hepatocellular carcinoma formation via remodeling ECM-receptor interaction pathway mediated by HMMR. Curr Gene Ther. 2024;24(3):249–63. https://doi.org/10.2174/0115665232274223231017052707.
43. Li T, Wang Y, Chen X, Cui H, Zhang L, Liu J, et al. Direct cytosolic delivery of siRNA conjugates: a paradigm in antiangiogenic therapy for choroidal neovascularization. ACS Nano. 2025;19(11):11249–62. https://doi.org/10.1021/acsnano.4c18924.
44. Lattanzi C, Bianchetto-Aguilera F, Donini M, Pettinella F, Caveggion E, Castellucci M, et al. Uncovering common transcriptional features shared by mature peripheral blood PMN-MDSCs and tumor-infiltrating neutrophils in humans. Oncoimmunology. 2025;14(1):2521396. https://doi.org/10.1080/2162402X.2025.2521396.
45. Li X, Tan Y, Liu B, Guo H, Zhou Y, Yuan J, et al. Mitochondrial lipid metabolism genes as diagnostic and prognostic indicators in hepatocellular carcinoma. Curr Genomics. 2023;24(2):110–27. https://doi.org/10.2174/1389202924666230914110649.
46. Zhou Y, Gu J, Yu H, Chen F, Long C, Maihemuti M, et al. Screening and identification of ESR1 as a target of Icaritin in hepatocellular carcinoma: evidence from bibliometrics and bioinformatic analysis. Curr Mol Pharmacol. 2024;17:e18761429260902. https://doi.org/10.2174/0118761429260902230925044009.
47. Sun XM, Luo ZN, Wang W, Hao CY, Li ZA, El-Ashram S, et al. Trichinella spiralis adult excretory-secretory antigen promotes peripheral regulatory T cell differentiation and attenuates experimental colitis via TGF-beta-like mechanisms. Parasit Vectors. 2025;18(1):240. https://doi.org/10.1186/s13071-025-06877-x.
48. Tay RE, Ho CM, Ang NDZ, Tay HC, Lopez DZ, Na QR, et al. Serotonin receptor 5-HT(2A) as a potential target for HCC immunotherapy. J Immunother Cancer. 2025. https://doi.org/10.1136/jitc-2024-011088.
49. Huang Y, Gao Z, Fan Z. Construction of a mitochondria-targeted NIR probe with large Stokes shift for real-time monitoring viscosity changes during ferroptosis. Spectrochim Acta A Mol Biomol Spectrosc. 2025;342:126488. https://doi.org/10.1016/j.saa.2025.126488.
50. Lai Y, Xiao W, Lei Z, Long H, Deng J, Wang Y, et al. Primer exchange reaction with cascade RNA transcription for highly specific detection of exosomal miRNA and liver cancer diagnosis. Anal Chem. 2025;97(7):4151–7. https://doi.org/10.1021/acs.analchem.4c06517.

Publisher's Note